YTHDF3-mediated m6A modification facilitates osteosarcoma progression through the FSP1-CoQ10-NAD(P)H axis to suppress ferroptosis

Wei Liu[1,2], Qingning Li[3], Nan Zhu[1,2], Shuo Zhang[1,2], Juehua Jing[1,2]*, Junfeng Zhan[1,2]*

[1]Department of Orthopaedics, The Second Affiliated Hospital of Anhui Medical University, Hefei, China
[2]Institute of Orthopaedics, Research Center for Translational Medicine, The Second Affiliated Hospital of Anhui Medical University, Hefei, China
[3]Emergency Department, Anhui No. 2 Provincial People's Hospital, Hefei, China

Submitted: 10 November 2023; **Accepted:** 11 April 2024
Online publication: 19 April 2024

Arch Med Sci
DOI: https://doi.org/10.5114/aoms/187043

***Corresponding authors:**
Junfeng Zhan
Juehua Jing
Department of Orthopaedics
The Second Affiliated Hospital of Anhui Medical University
Institute of Orthopaedics Research Center for Translational Medicine
The Second Affiliated Hospital of Anhui Medical University
Hefei 230601, China
E-mail:
Zhanjunfeng0901@163.com
jjhhu@sina.com

Abstract

Introduction: Osteosarcoma (OS) remains a formidable malignancy, characterized by its relentless nature and limited therapeutic interventions. YTHDF3, a key reader protein recognizing m6A-modified mRNAs, has attracted considerable attention due to its prominent role in cancer biology. This study investigated the relationship between YTHDF3, a vital RNA modification reader protein, m6A RNA modification, and the FSP1-CoQ10-NADPH metabolic pathway in the pathogenesis of OS.
Material and methods: Firstly, we procured tissue specimens and corresponding non-cancerous tissues from 10 OS patients and cultured OS cell lines. Then, we established a ferroptosis model in OS cells through treatment with RSL3 to reveal the relation between YTHDF3 and ferroptosis.
Results: Clinical evaluation of OS samples revealed a notable upsurge in the expression of YTHDF3 and the concurrent overexpression of ferroptosis-related proteins. *In vitro* experiments suggested that YTHDF3 potentially facilitated FSP1 mRNA translation through an m6A-dependent mechanism, subsequently inhibiting ferroptosis via the FSP1-CoQ10-NADPH pathway, thereby promoting OS progression. These compelling findings underscore the promise of targeting the YTHDF3-FSP1 axis as an innovative and potentially transformative therapeutic strategy for the treatment of OS.
Conclusions: This study not only enhances our understanding of ferroptosis regulation but also sheds light on the significance of YTHDF3 and FSP1 as potential targets for therapeutic intervention in OS, offering new prospects for cancer treatment strategies.

Key words: osteosarcoma, YTHDF3, m6A modification, FSP1, ferroptosis.

Introduction

Osteosarcoma (OS), originating from primitive mesenchymal cells, represents a primary malignant musculoskeletal neoplasm. Due to its pronounced malignancy, early metastasis, intrinsic resistance, high disability rate, elevated mortality, and exceedingly poor prognosis, OS presents a disheartening therapeutic outlook [1, 2]. Comprehensive elucidation of its pathogenesis is urgently warranted, offering novel avenues for the progression of innovative therapies. In recent times, at-

tention has turned to ferroptosis, a unique form of iron-dependent regulated cell death, distinct from classical modes such as necrosis, apoptosis, and autophagy, as a potential avenue of interest [3, 4]. Emerging findings have spotlighted apoptosis-inducing factor mitochondria-associated 2 (AIFM2), namely ferroptosis suppressor protein 1 (FSP1) or programmed cell death protein 3 (PRG3), as an endogenous inhibitor of ferroptosis, capable of impeding phospholipid peroxidation and cellular iron-driven demise via the FSP1-CoQ10-NADPH pathway [5–7]. Meanwhile, extracellular vesicle-derived miR-4443 modulates ferroptosis by targeting METTL3 in non-small cell lung cancer (NSCLC) to suppress FSP1 m6A modification [8]. However, the involvement of FSP1 in OS remains uncharted territory in current literature.

N6-methyladenosine (m6A) is the most prevalent and ubiquitous mRNA modification, exercising pivotal roles and functionalities throughout a spectrum of biological processes. An accumulating body of evidence underscores the participation of m6A regulatory factors in various cancers, exerting significant roles in tumor cell proliferation and metastasis [9–11]. Reports have highlighted ALKBH5, a pivotal RNA demethylase, which, via an m6A-YTHDF2-dependent mechanism, orchestrates STAT3 activity, consequently impacting OS proliferation and oncogenicity [12]. Likewise, METTL14, serving as an m6A RNA methyltransferase, contributes to OS progression and all-trans-retinoic acid resistance by modulating MN1 stability and translation efficiency [13]. Consequently, the targeting of specific gene m6A modifications emerges as a promising strategy for cancer therapy.

The YTH domain family protein 3 (YTHDF3) holds a pivotal role in governing the translation of mRNA modified by N6-methyladenosine (m6A), and it exerts its regulatory influence on the degradation of methylated mRNA through an m6A methylation-dependent pathway [14]. YTHDF3 has been evidenced to contribute to the progression of several tumor types, including gastric [15] and colorectal cancers [16]. Nevertheless, the functional implications of YTHDF3 during ferroptosis in cancer cells remain uncharted.

In this study, we investigated the role of YTHDF3 in OS cell death and evaluated its regulatory effect on FSP1 m6A modification. Our findings provide novel evidence for the prospective therapeutic targeting of YTHDF3 in the management of OS.

Material and methods

Tissue collection

From September 2017 to December 2020, we collected pathological specimens from OS patients at The Second Hospital Affiliated with Anhui Medical University. Additionally, adjacent non-cancerous tissues were obtained after excluding patients with coexisting malignancies, cardiovascular disorders or psychiatric disorders. We successfully procured OS tissue specimens and corresponding non-cancerous tissues from 10 patients. Pathological assessment by two pathologists confirmed the diagnosis of OS. For preservation, tissue samples were immediately frozen in liquid nitrogen and kept at –80°C. The Ethics Committee of this hospital approved the study in accordance with ethical standards. Informed consent was acquired from all patients and their families, ensuring their understanding of the study's purpose and procedures.

Cell culture and treatment

The Chinese Academy of Sciences' Cell Bank (Shanghai, China) provided the OS cell lines U2OS and Mg-63. 10% fetal bovine serum was added to Dulbecco's Modified Eagle Medium (DMEM), and the cells were grown in this medium while being kept at 37°C and 5% CO_2. To induce iron-dependent cell death, cells were treated with RSL3 (Sigma). An equal volume of dimethyl sulfoxide (DMSO) without the drug was applied to the control cells. YTHDF3-sh, YTHDF3-OE, FSP1-sh, and FSP1-OE plasmids were obtained from GeneChem (Shanghai, China). For 48 h, oligonucleotides were combined with Lipofectamine 2000. Subsequently, cells were used for further study.

RNA extraction and cDNA synthesis

Total RNA was collected from tissues and cells by Trizol reagent (Thermo Fisher Scientific, USA) according to the standard protocol. Subsequently, 1.5 µg of RNA was utilized for cDNA synthesis employing the First Strand cDNA Synthesis Kit (Takara, Japan). For quantitative analysis of gene expression, the synthesized cDNA was utilized. SYBR Green Mix (Thermo Fisher Scientific, USA) was employed to perform the real-time polymerase chain reaction (PCR), and the expression levels of the target genes were determined by the $2^{-\Delta\Delta Ct}$ method with GAPDH as the internal control.

Western blot (WB)

The WB was performed in accordance with standard procedures [17]. Cells underwent lysis in RIPA buffer (Beyotime, China), and denatured samples (30 µg) were loaded onto 10% acrylamide gels. After SDS-PAGE, proteins were transferred to polyvinylidene difluoride membranes and blocked with 5% skim milk for 2 h. The membranes were treated with anti-YTHDF3 (Abcam, #ab220161), anti-FSP1 (Abcam, #1978968), anti-GPX4 (Abcam, #ab125066), and anti-β-ACTIN (Cell Signaling Technology, #2128) for an overnight period at

4°C. Membranes were probed with HRP-conjugated secondary antibodies (anti-rabbit, Cell Signaling Technology, #7074) for 1 h indoors following primary antibody incubation. Pierce ECL Western Blotting Substrate from Thermo Fisher Scientific (USA) was used to identify signals.

Cell count Kit-8 (CCK-8)

Cell viability was evaluated by the CCK-8 assay (Beyotime, China) [18]. The cells were initially seeded at a density of 1×10^5 cells per well in 96-well plates. On the second day, after 6-hour transfection, the culture medium supplemented with 10 µM/l RSL3 was introduced, followed by cell incubation for 24, 48, 72, and 96 h. Following this, CCK-8 (10 µl) was added to each well, and the cell plates were incubated at 37°C for 1 h. Absorbance was measured at 450 nm using a microplate reader (Model 680 Microplate Reader; Bio-Rad, USA).

Apoptosis

Apoptosis in cells was assessed using the V-FITC Membrane Protein Apoptosis Assay Kit (CA1020, Solarbio, Beijing, China) [19]. 1 ml of cell suspension (1×10^6 cells/ml) underwent centrifugation at 1000*g* for 5 min at 4°C. After discarding the supernatant, 1 ml of precooled PBS buffer was added. The mixture underwent subsequent centrifugation, and the supernatant was discarded, with these steps being repeated twice. Following this, cells were resuspended in 100 µl of binding buffer, stained with 5 µl of Annexin V-FITC in the dark for 15 min, and then 5 µl of propidium iodide (PI) in the dark for 5 min. The cell suspension was then analyzed using the NovoCyte flow cytometer (Agilent Technologies) to quantify apoptotic cells based on fluorescence emissions.

Enzyme-linked immunosorbent assay (ELISA)

The CoQ10 levels were measured utilizing the CoQ10 ELISA Kit (CUSABIO, CSB-E14081h) [20]. Following the specified treatments, PBS was used to homogenize the collected cells, which were then centrifuged at 10000*g* for 10 min. The supernatant was loaded onto the assay plate and thoroughly mixed with the HRP-conjugated reagent. After that, the mixture was incubated for 37 min at 40°C. After five washes with wash buffer, TMB substrate was added to each well, and the plate was incubated at 20°C in darkness for 37 min. Finally, stop solution was added, and the plate was read at 450 nm to measure the absorbance.

MDA and NADPH measurement

MDA (malondialdehyde) levels were quantified using the TBA assay kit (A003-1-2, Nanjing Jiancheng Bioengineering Institute) following the manufacturer's instructions [21]. Intracellular NADPH levels were determined using the Coenzyme II (NADP/NADPH) content test kit (A115-1-1, Nanjing Jiancheng Bioengineering Institute) in accordance with the manufacturer's instructions [22].

Reactive oxygen species (ROS) detection and analysis

ROS levels were detected by an ROS detection kit with 6-carboxy-2′,7′-dichlorodihydrofluorescein diacetate (DCFHDA) from Thermo Fisher Scientific [23]. Cells were treated and then exposed to DCFHDA, which becomes fluorescent upon oxidation by ROS. Fluorescence intensity, indicating ROS levels, was monitored and quantified using a flow cytometer as per the manufacturer's instructions.

Iron determination

Cellular iron concentrations relative to Fe^{2+} and Fe^{3+} were evaluated using the Iron Detection Assay Kit (ab83366, Abcam) [24]. Cells were homogenized in a 4–10 volume of iron determination buffer. To remove insoluble particles, the homogenate was centrifuged at 16000*g* for 10 min. The resultant supernatant was transferred to a 96-well plate and then diluted with assay buffer to a final volume of 100 µl. 100 µl of iron probe was added after the reaction mixture had been incubated at 37°C for 30 min. The reaction mixture was then incubated at 37°C for an additional 60 min. Following incubation, the absorbance was measured at 593 nm using a microplate reader.

Transmission electron microscopy

Cells were fixed in 2.5% glutaraldehyde solution with Millonig's phosphate buffer (pH = 7.3). After three washes with Millonig's phosphate buffer, cells were incubated in 1% osmium tetroxide for 1 h, followed by three washes with Millonig's phosphate buffer. Samples were dehydrated in increasing concentrations of acetone, embedded in a 1 : 1 mixture of acetone and resin for 12 h, polymerized overnight at 37°C in 100% resin, and further polymerized for 12 h at 60°C. Ultra-thin sections were cut using a Leica Ultracut microtome (Leica EM UC7), stained with uranyl acetate and lead nitrate, and examined in a Hitachi HT-7700 electron microscope [20].

Mitochondrial membrane potential (MMP) assessment

MMP was evaluated with the JC-1 Mitochondrial Membrane Potential Detection Kit (M8650, Solarbio, Beijing, China) [25]. Cells were washed before being exposed to the JC-1 working solution

for 37 min at 30°C in a CO_2 incubator. Live cells were photographed using a confocal laser scanning microscope after incubation. Meanwhile, cells treated with CCCP as per instructions served as the negative control for MMP assessment. In the presence of a high MMP, JC-1 aggregates glow red whereas JC-1 monomers fluoresce green. Using ImageJ software created by Wayne Rasband, MD, USA, the fast exposure confocal images were measured for the average fluorescence intensity of particular locations.

m6A RNA methylation quantification

The m6A RNA methylation levels were measured using the EpiQuik m6A RNA Methylation Quantitative Assay Kit (Colorimetric Method, Biyuntian Biotechnology, China) following instructions [26]. For each assay well, 6 ng of RNA and the appropriate antibody were added. 200 nm absorbance values were measured and computed as directed by the manufacturer's protocol.

mRNA stability analysis

To investigate mRNA stability, the actinomycin D (Act D) chase method was employed, as described previously [27].

Tumor xenografting

Vital River Laboratory (China) provided six-week-old BALB/c nude mice, which were raised under the recommended, pathogen-free conditions. The left flank fat pad of the nude mice was injected with 1×10^6 U2OS cells stably transfected with siYTHDF3 or shNC (n = 6 per group). After a 30-day growth period, the mice were euthanized, and the tumors were prepared for immunostaining and H&E staining [28].

Tissue processing and histological analysis

Tissues were fixed in 4% paraformaldehyde, dehydrated, and subsequently embedded in paraffin blocks. Sections were cut from the blocks and utilized for both hematoxylin and eosin (HE) staining [29] and immunohistochemistry (IHC) [30]. The sections in IHC were kept with primary antibodies, including anti-YTHDF3 (Abcam, ab220161), anti-FSP1 (Abcam, ab197896), and anti-GPX4 (Abcam, ab125066). These primary antibodies were selected to target specific proteins of interest in the study. All images were acquired using an Olympus microscope (Olympus, Japan).

Statistical analysis

One-way ANOVA with Tukey's test or the t-test was used to assess the experimental data (n = 3, $p < 0.05$). Representative images were chosen from multiple sections. IHC staining intensity was statistically evaluated using the Mann-Whitney U test. Results are presented as mean ± SD/SEM.

Results

Clinical assessment reveals m6A modification and ferroptosis-related proteins in OS

To investigate the mechanisms of m6A modification in clinical contexts, we explored 10 OS patient specimens alongside 10 adjacent non-tumor samples. As illustrated in Figure 1, upregulated YTHDF3 in OS patients was revealed. Moreover, ferroptosis-associated proteins, including glutathione peroxidase 4 (GPX4) and FSP1, were markedly elevated in OS patients. Overall, these findings suggest the involvement of m6A modification and ferroptosis in OS, providing insights into potential underlying mechanisms.

RSL3-mediated ferroptosis induction and YTHDF3 regulation in OS cells

RSL3, a classical small molecule known to induce ferroptosis by inhibiting GPX4's peroxidase activity, was investigated for appropriate intervention conditions [31]. Concentration gradient and time-point experiments were conducted by subjecting cells to gradient concentrations of RSL3 for 24–48–72 h. The IC_{50} of RSL3 in U2OS was approximately 11.90–5.823–4.038 μM (Figure 2 A), while in Mg-63 cells, it was about 22.59–9.445–7.104 μM (Figure 2 B). Further experiments employed 5 μM RSL3 treatment for 48 h in U2OS cells and 10 μM RSL3 for 48 h in Mg-63 cells to establish ferroptosis models. Transmission electron microscopy revealed characteristic ultrastructural changes associated with ferroptosis after RSL3 treatment, including mitochondrial shrinkage and pronounced chromatin decondensation in the nucleus (Figure 2 C). Consistent with expectations, qRT-PCR and WB analysis demonstrated significant suppression of YTHDF3, GPX4, and FSP1 mRNA and protein levels upon RSL3 treatment (Figures 2 D–H).

Modulation of YTHDF3 alters ferroptosis susceptibility in OS cells

Lentivirus-mediated vectors targeting YTHDF3 (shYTHDF3) and carrying YTHDF3 gene (OE-YTHDF3) were introduced into U2OS and Mg-63 OS cell lines. qRT-PCR confirmed knockdown and overexpression efficiency (Figures 3 A, B). CCK-8 assays revealed increased proliferation in OE-YTHDF3 cells compared to OE-NC, while shYTHDF3 cells exhibited decreased proliferation compared to Sh-NC (Figure 3 C). Flow cytometry-based apoptosis detection demonstrated reduced apoptosis

rates in OE-YTHDF3 cells and elevated rates in shYTHDF3 cells (Figure 3 D). ELISA results displayed reduced malondialdehyde (MDA) levels in YTHDF3-overexpressing cells, suggesting lower lipid oxidation and enhanced oxidative damage (Figure 3 E). Conversely, shYTHDF3 cells exhibited elevated MDA levels (Figure 3 E). Flow cytometry analysis revealed that YTHDF3 overexpression significantly lowered ROS levels, while shYTHDF3 significantly increased ROS levels (Figure 3 F). JC-1 staining indicated that YTHDF3 overexpression elevated mitochondrial membrane potential, while YTHDF3 knockdown reduced it (Figure 3 G). Moreover, the overexpression of YTHDF3 led to a notable reduction in intracellular levels of both Fe^{2+} and Fe^{3+}, while conversely, the knockdown of YTHDF3 resulted in opposite results (Figures 3 H–I).

YTHDF3 modulation affects FSP1, GPX4, CoQ10, and NADPH levels in OS cells

YTHDF3 overexpression remarkably increased the mRNA and protein expression of FSP1 and GPX4 in OS cells, while YTHDF3 knockdown notably suppressed them (Figures 4 A–D). Transmission electron microscopy revealed that YTHDF3 overexpression attenuated RSL3-induced alterations, including mitochondrial shrinkage, chromatin decondensation, and nuclear changes (Figure 4 E). Conversely, YTHDF3 knockdown exacerbated RSL3-induced ferroptosis morphological features

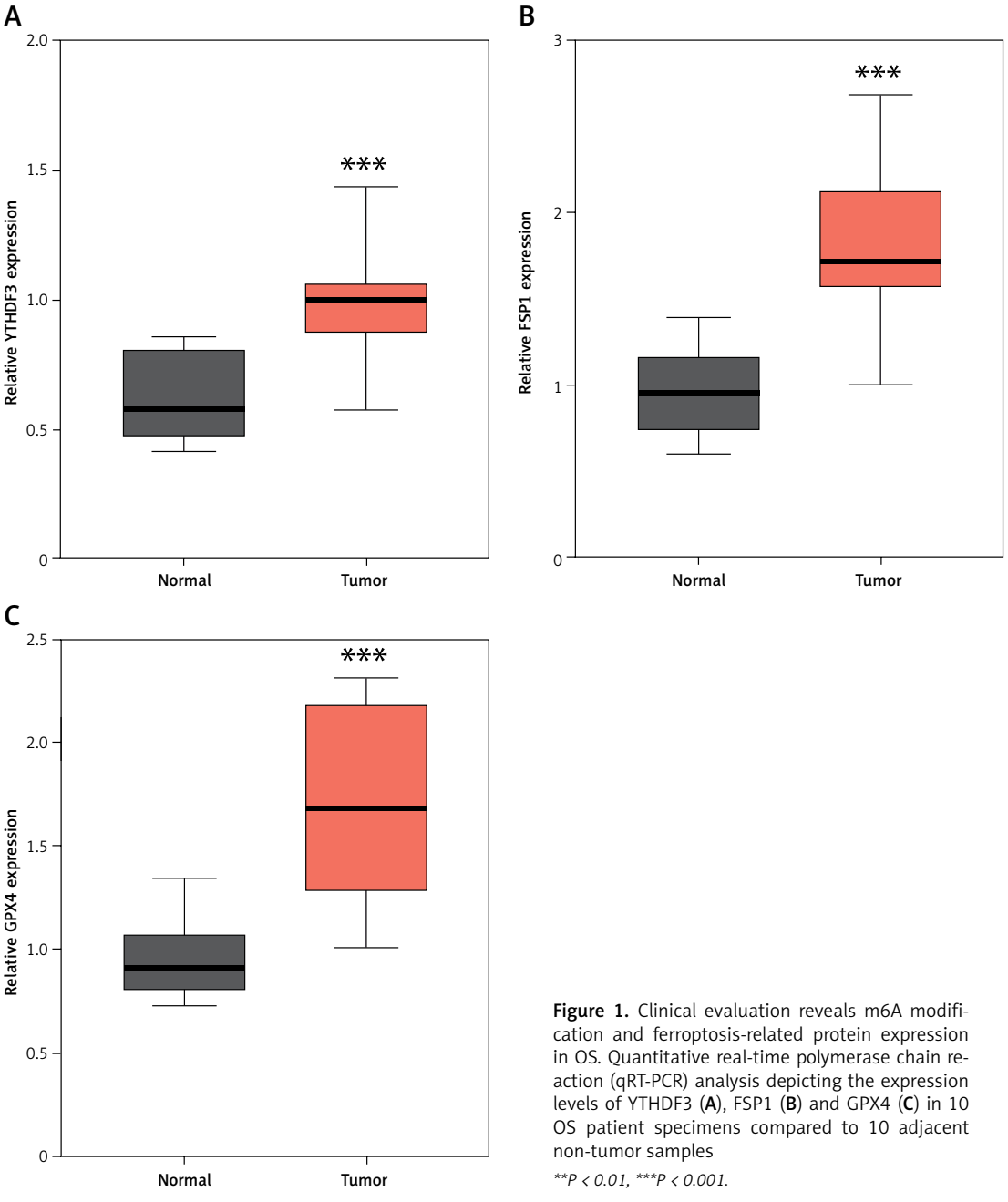

Figure 1. Clinical evaluation reveals m6A modification and ferroptosis-related protein expression in OS. Quantitative real-time polymerase chain reaction (qRT-PCR) analysis depicting the expression levels of YTHDF3 (**A**), FSP1 (**B**) and GPX4 (**C**) in 10 OS patient specimens compared to 10 adjacent non-tumor samples

***P < 0.01, ***P < 0.001.*

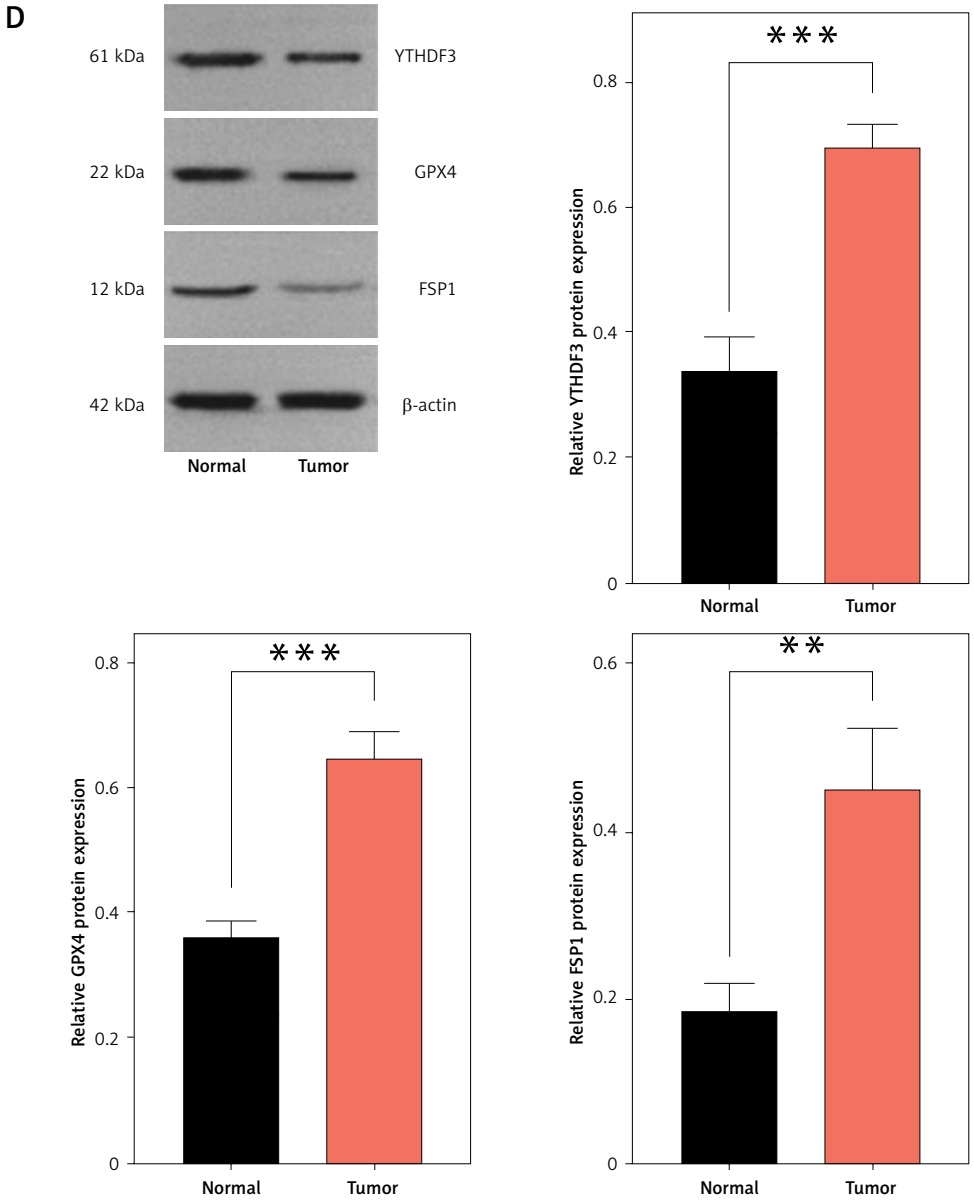

Figure 1. Cont. Western blot analyses displaying protein expression levels of YTHDF3, GPX4, and FSP1 in 10 OS patient specimens along with 10 adjacent non-tumor samples (**D**)

***P < 0.01, ***P < 0.001.*

(Figure 4 F). ELISA results demonstrated elevated CoQ10 levels upon YTHDF overexpression (Figure 4 F), whereas shYTHDF cells showed reduced CoQ10 levels (Figure 4 G). YTHDF3 overexpression increased NADPH levels in OS cells, while YTHDF3 knockdown yielded the opposite effect (Figure 4 H). These findings illuminate the intricate role of YTHDF3 in regulating FSP1, GPX4, CoQ10, and NADPH levels, contributing to the modulation of ferroptosis susceptibility in OS cells.

Impact of FSP1 modulation on ferroptosis susceptibility in OS cells

Lentivirus-mediated vectors targeting FSP1 (shFSP1) and carrying the FSP1 gene (OE-FSP1) were introduced into U2OS and Mg-63 OS cell lines, followed by qRT-PCR to validate knockdown and overexpression efficiency (Figures 5 A, B). CCK-8 assays demonstrated enhanced proliferation in OE-FSP1 cells compared to OE-NC, while shFSP1 cells exhibited increased proliferation compared to Sh-NC (Figure 5 C). Cell apoptosis analysis revealed reduced apoptosis rates in OE-FSP1 cells and elevated rates in shFSP1 cells (Figure 5 D). ELISA results indicated reduced MDA levels upon FSP1 overexpression (Figure 5 E), whereas shFSP1 cells showed higher MDA levels (Figure 5 E). Flow cytometry analysis demonstrated significantly lowered ROS levels in FSP1-overexpressing cells, while shFSP1 significantly increased ROS levels

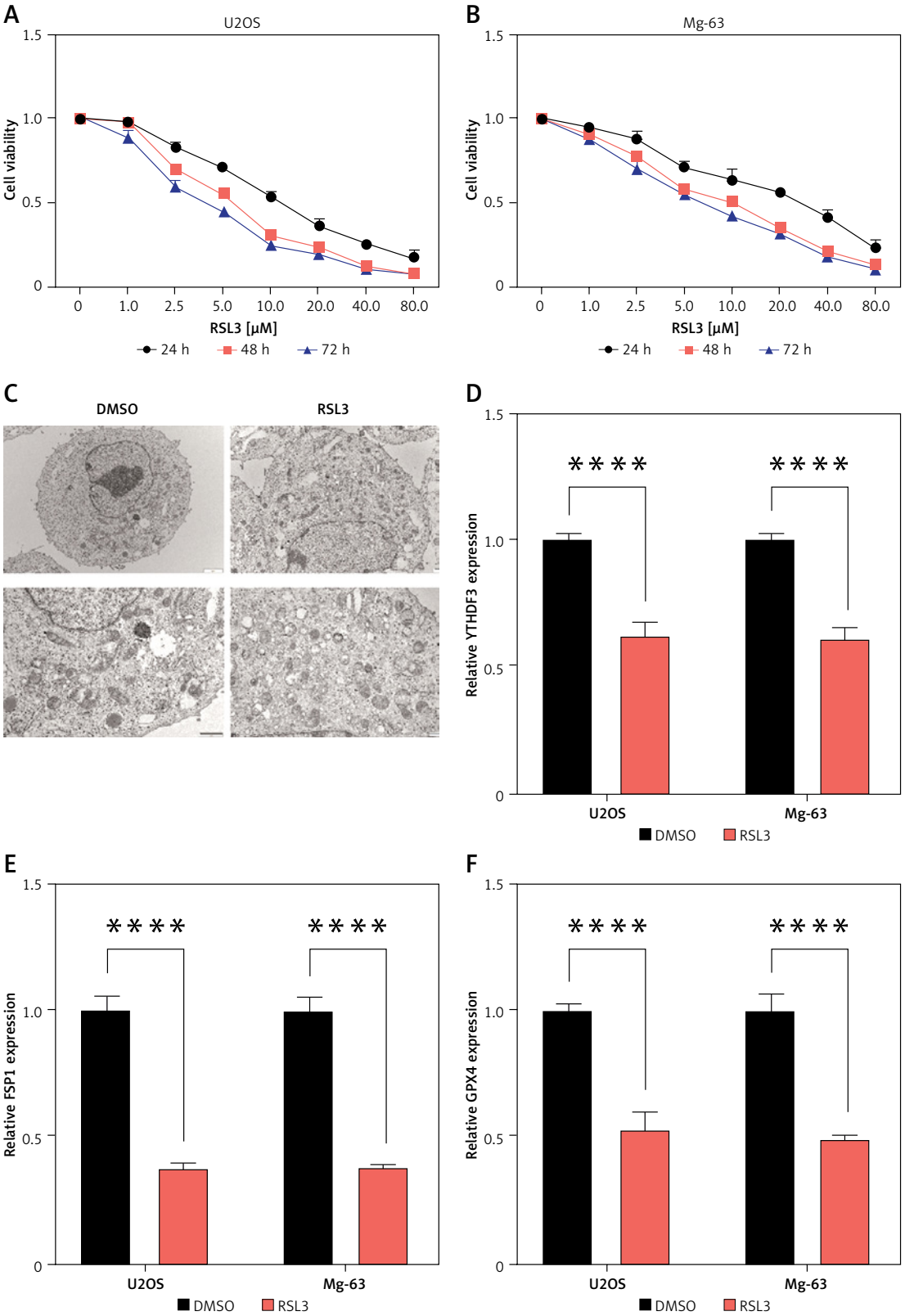

Figure 2. Investigation of RSL3-mediated ferroptosis induction and YTHDF3 regulation in OS cells. **A** – Concentration-response experiment depicting the IC_{50} values of RSL3 in U2OS cells, measured at approximately 11.90–5.823–4.038 μM. **B** – Concentration-response experiment revealing the IC_{50} values of RSL3 in Mg-63 cells, recorded at approximately 22.59–9.445–7.104 μM. **C** – Transmission electron microscopy images showing characteristic ultrastructural changes associated with ferroptosis following RSL3 treatment. **D** – qRT-PCR analysis revealing the modulation of YTHDF3 mRNA expression levels (**E**), GPX4 (**F**)

*****P < 0.0001.*

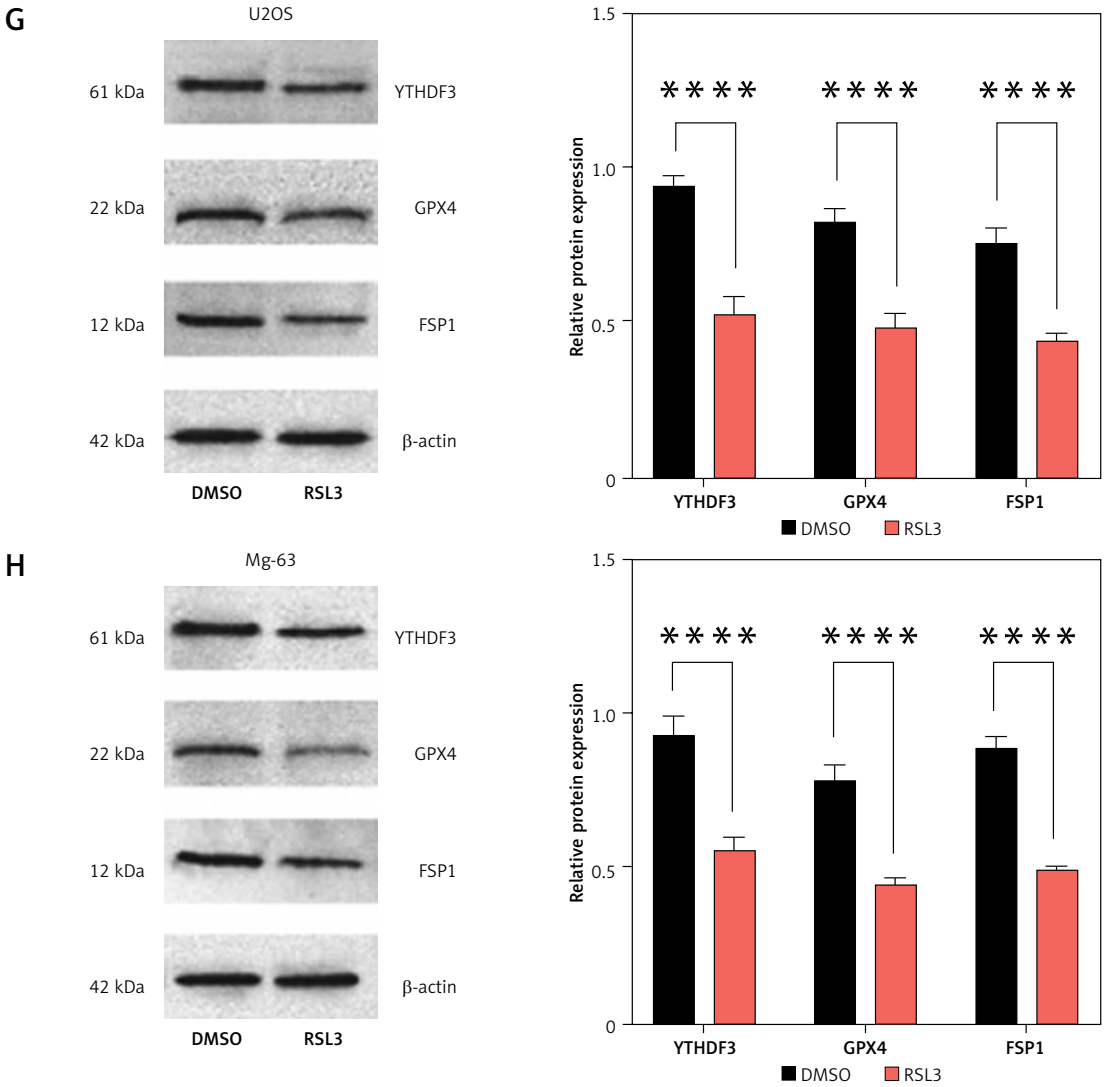

Figure 2. Cont. FSP1 (**G**) in response to RSL3 treatment. **H** – Western blot analysis displaying the alterations in YTHDF3, GPX4, and FSP1 protein expression levels in response to RSL3 treatment

*****P < 0.0001.*

(Figure 5 F). JC-1 staining revealed that FSP1 overexpression elevated mitochondrial membrane potential, while FSP1 knockdown reduced it (Figure 5 G). Moreover, FSP1 overexpression reduced cellular Fe^{2+} and Fe^{3+} levels, whereas FSP1 knockdown yielded opposite results (Figures 5 H–I).

FSP1 modulation influences GPX4 levels and ferroptosis susceptibility in OS cells

We observed significant upregulation of GPX4 mRNA and protein levels upon FSP1 overexpression in OS cells, while FSP1 knockdown led to pronounced suppression of GPX4 levels without affecting YTHDF3 expression (Figures 6 A–D). Transmission electron microscopy demonstrated that FSP1 overexpression mitigated RSL3-induced alterations including mitochondrial shrinkage, chromatin decondensation, and nuclear changes (Figure 6 E). Conversely, FSP1 knockdown exacerbated RSL3-induced ferroptosis morphological features (Figure 6 F). ELISA results indicated increased CoQ10 levels upon FSP1 overexpression, whereas shFSP1 cells exhibited lower CoQ10 levels (Figure 6 G). FSP1 overexpression also elevated NADPH levels in OS cells, while FSP1 knockdown yielded the opposite effect (Figure 6 H).

YTHDF3-mediated m6A modification of FSP1 modulates ferroptosis in OS

Given YTHDF3's role in regulating ferroptosis in OS cells, our study aimed to explore the potential mechanisms underlying YTHDF3-mediated ferroptosis regulation. Functional experiments revealed the involvement of FSP1 in modulating ferroptosis in OS. As depicted in Figures 7 A, B, RSL3-induced treatment significantly reduced

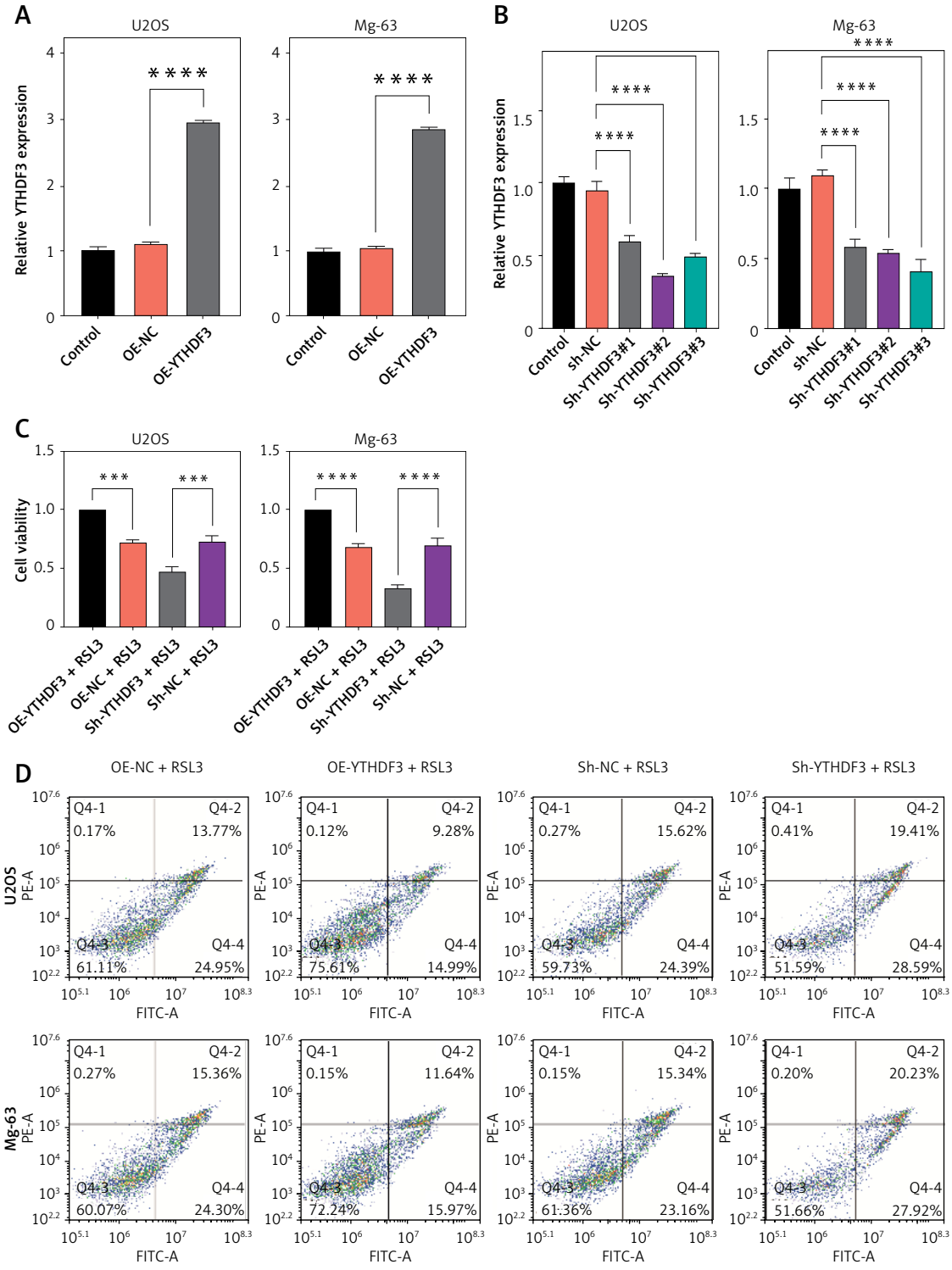

Figure 3. Impact of YTHDF3 modulation on ferroptosis susceptibility in OS cells. **A**, **B** – qRT-PCR validation confirming the efficiency of knockdown and overexpression strategies for the respective targets. **C** – Cell Counting Kit-8 (CCK-8) assays depict the proliferative capacity of OE-YTHDF3 cells relative to OE-NC, and proliferation in shYTHDF3 cells compared to Sh-NC controls. **D** – Flow cytometry-based apoptosis analysis reveals the apoptotic rates in OE-YTHDF3 and shYTHDF3 cells

***P < 0.01, ***p < 0.001, ****p < 0.0001.*

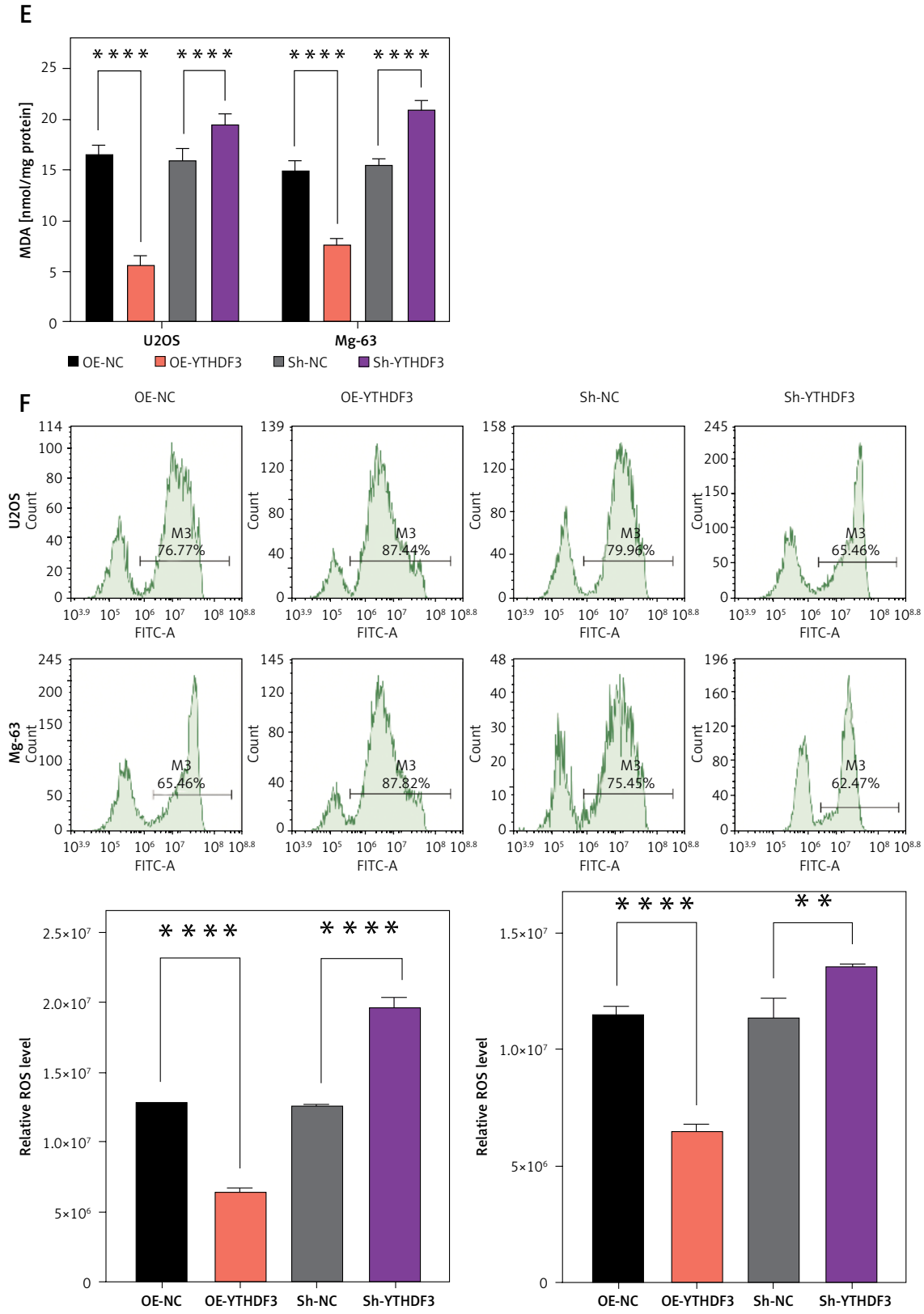

Figure 3. Cont. **E** – Enzyme-linked immunosorbent assay (ELISA) results demonstrate alterations in malondialdehyde (MDA) levels in YTHDF3 overexpression and YTHDF3 knockdown. **F** – Flow cytometry analysis illustrates the impact of YTHDF3 overexpression and knockdown on intracellular reactive oxygen species (ROS) levels. **G** – JC-1 staining provides visual representation of mitochondrial membrane potential changes in response to YTHDF3 overexpression and knockdown. **H**, **I** – Alterations in cellular Fe^{2+} and Fe^{3+} levels upon YTHDF3 overexpression and knockdown through iron assay kit

***P < 0.01, ***p < 0.001, ****p < 0.0001.*

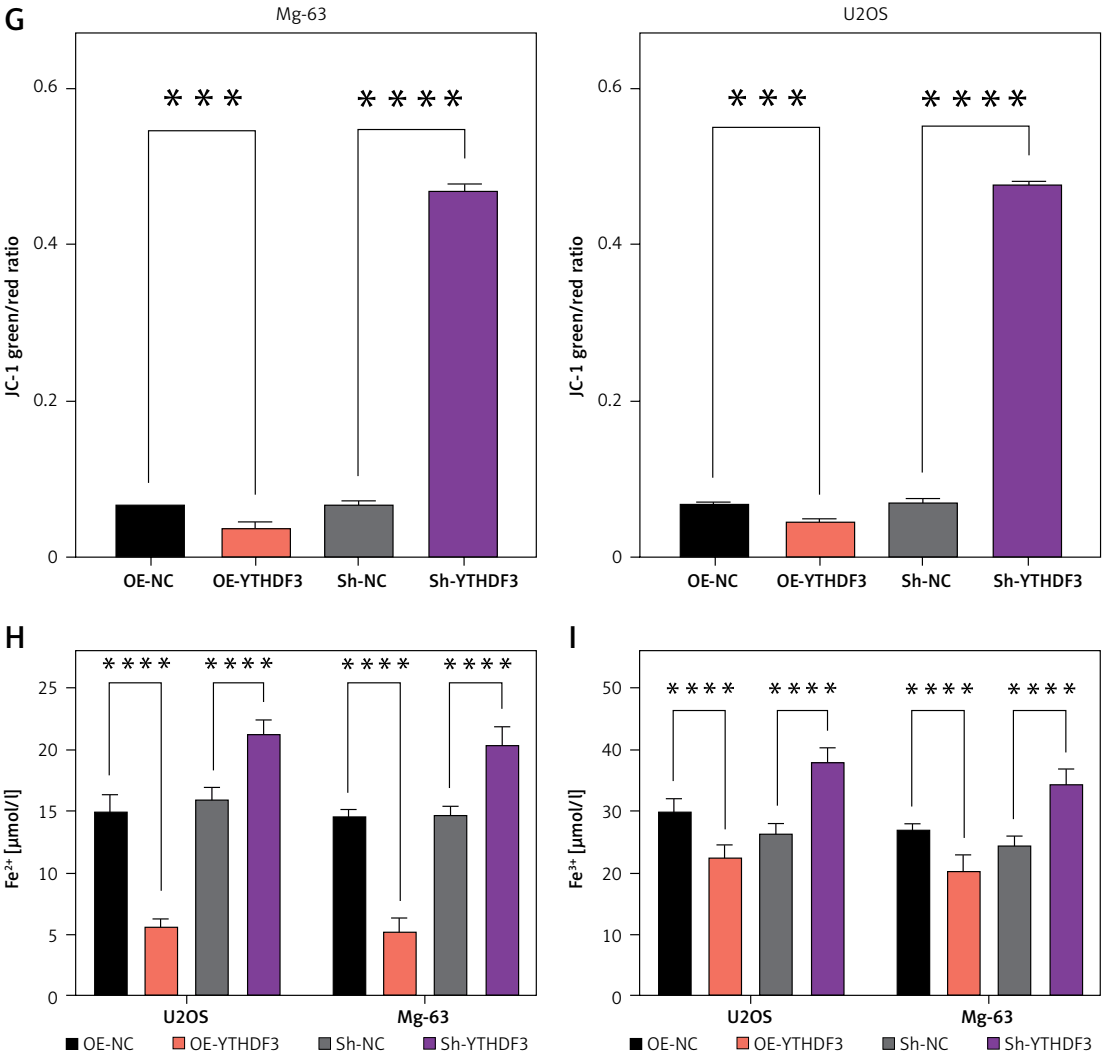

Figure 3. Cont. **G** – JC-1 staining provides visual representation of mitochondrial membrane potential changes in response to YTHDF3 overexpression and knockdown. **H, I** – Alterations in cellular Fe^{2+} and Fe^{3+} levels upon YTHDF3 overexpression and knockdown through iron assay kit

***P < 0.01, ***p < 0.001, ****p < 0.0001.*

the m6A methylation level of FSP1 in OS cells. To investigate YTHDF3's regulatory impact on FSP1 mRNA, RNA decay analyses were conducted in OS cells. The results demonstrated that YTHDF3 overexpression markedly elevated FSP1 mRNA levels following Act D treatment (Figure 7 C), while YTHDF3 silencing inhibited FSP1 mRNA levels upon Act D treatment (Figure 7 D).

YTHDF3 mediates FSP1-regulated ferroptosis in OS cells

In order to confirm FSP1 as the mediator of YTHDF3-regulated cell ferroptosis, rescue experiments were conducted. The knockdown of YTHDF3 significantly inhibited GPX4 and FSP1 levels in U2OS and Mg-63 cells, while overexpression of FSP1 restored the levels of GPX4 and FSP1, without affecting YTHDF3 (Figures 8 A–D). As shown in Figure 8 E, sh-YTHDF3 inhibited the proliferation and induced apoptosis of U2OS and Mg-63 cells, whereas overexpression of FSP1 reversed these effects, restoring cell proliferation and inhibiting apoptosis (Figures 8 E, F). Over-expressed FSP1 attenuated the accumulation of MDA, ROS, Fe^{2+}, and Fe^{3+} induced by sh-YTHDF3 (Figures 8 G, H, J, K). Moreover, FSP1 overexpression restored the decreased mitochondrial membrane potential caused by sh-YTHDF3 (Figure 8 I). Transmission electron microscopy revealed that YTHDF3 knockdown aggravated the ferroptosis features induced by RSL3, including mitochondrial shrinkage and chromatin decondensation, while FSP1 overexpression alleviated these morphological changes (Figure 8 L). Furthermore, sh-YTHDF3 significantly inhibited CoQ10 and NADPH levels in OS cells, while FSP1 overexpression restored these levels (Figures 8 M, N). These results collectively em-

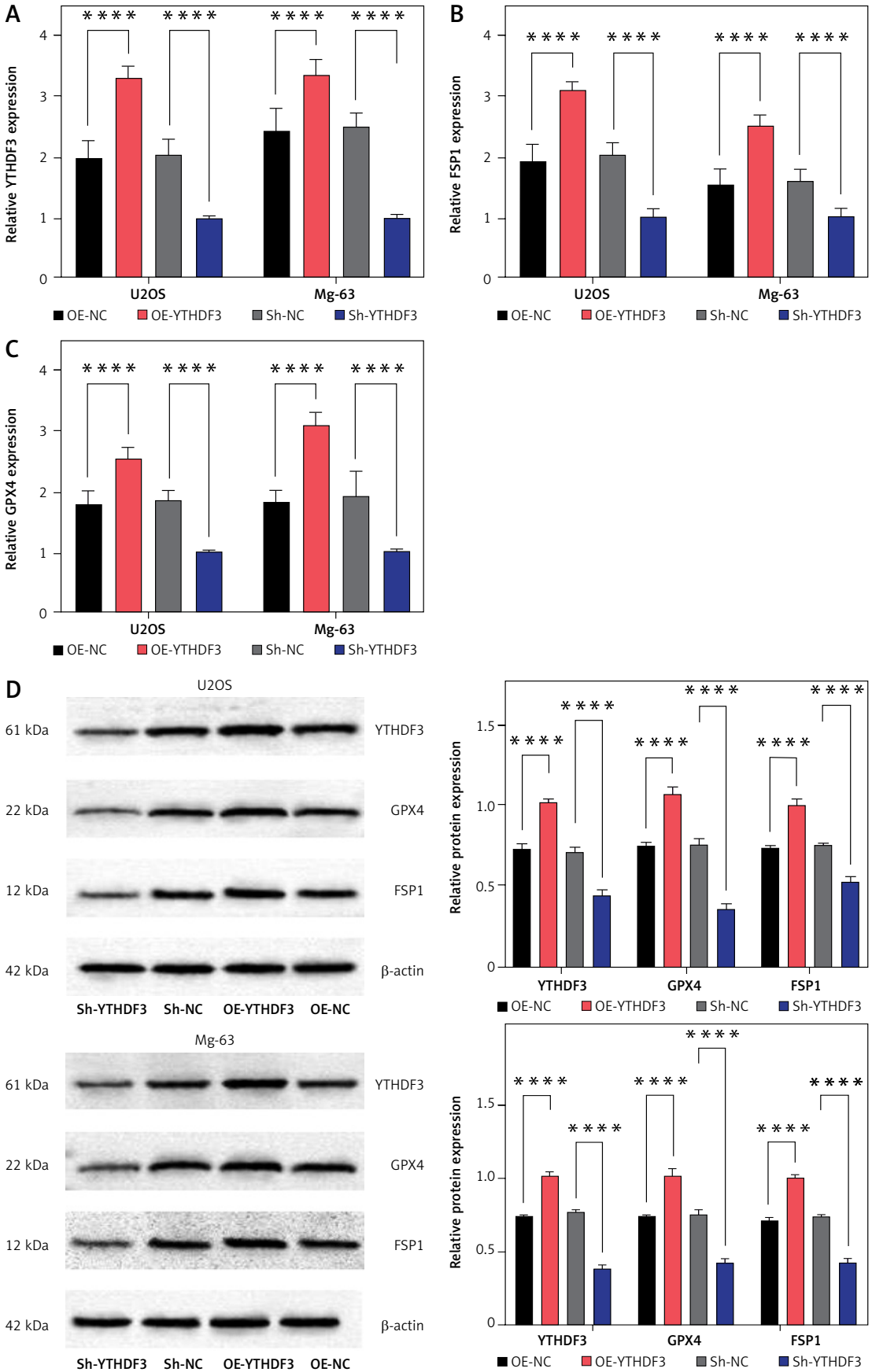

Figure 4. Influence of YTHDF3 modulation on FSP1, GPX4, CoQ10, and NADPH levels in OS cells. **A–D** – qRT-PCR and Western blot confirm YTHDF3's regulation of FSP1 and GPX4 in OS cells

***P < 0.01, ****p < 0.0001.*

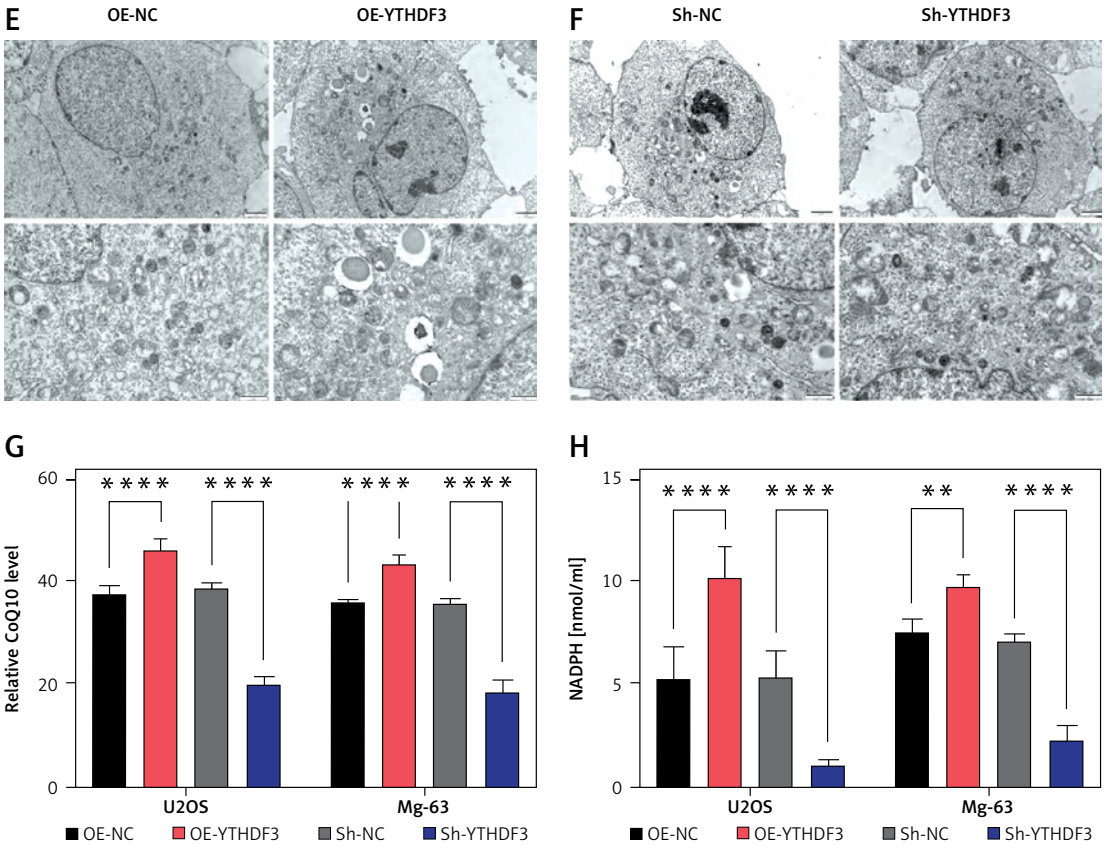

Figure 4. Cont. **E** – Transmission electron microscopy images reveal YTHDF3 overexpression's counteraction of RSL3-induced ferroptosis-associated morphological changes. **F** – Transmission electron microscopy images depict YTHDF3 knockdown's attenuation of RSL3-induced ferroptosis-associated morphological alterations. CoQ10 (**G**) and NADPH (**H**) level were determined upon YTHDF3 overexpression and knockdown

***P < 0.01, ****p < 0.0001.*

phasize the role of FSP1 as a pivotal downstream effector of YTHDF3 in regulating ferroptosis in OS cells.

Implications of YTHDF3 in regulating FSP1-CoQ10-GAPDH axis and ferroptosis

In the *in vivo* investigation, we subcutaneously implanted sh-YTHDF3 U2OS cells into mice. Histopathological analysis showed that the tumor pathology changes in the YTHDF3 knockdown group showed sparsely arranged and impaired texture compared with the control group, which improved the tumor pathology of the xenografts (Figure 9 A). IHC results showed that the percentage of YTHDF3, GPX4, and FSP1-positive cells in the sh-YTHDF3 group was lower than about half of that in the sh-NC group (Figures 9 B–E). qRT-PCR and WB analysis further confirmed that YTHDF3 knockdown significantly inhibited FSP1 and GPX4 levels (Figures 9 F–I). Notably, YTHDF3 knockdown led to the elevation of MDA, ROS, Fe^{2+}, and Fe^{3+} levels in the tumor microenvironment (Figures 9 J–M). Additionally, sh-YTHDF3 markedly suppressed CoQ10 and NADPH levels in OS tumors (Figures 9 N, O).

Discussion

In recent years, m6A modification has emerged as a pivotal post-transcriptional regulatory mechanism, exerting far-reaching effects on various cellular processes, including gene expression, RNA stability, and protein translation [32–34]. Growing evidence underscores the intricate connection between dysregulated m6A modifications and tumorigenesis [35, 36]. YTHDF3, a key reader protein recognizing m6A-modified mRNAs, has attracted considerable attention due to its prominent role in cancer biology [37, 38]. Research has revealed that YTHDF3 induces translation of m6A-enriched transcripts, thereby facilitating brain metastasis in breast cancer [39]. In ocular melanoma, YTHDF3 enhances CTNNB1 translation, intensifying the oncogenicity of cancer stem-like cells [40].

Herein, we initially measured YTHDF3 mRNA expression in OS and normal tissues. It was found that YTHDF3 levels were remarkably high in tumor tissues, supporting earlier observations. To delineate the functional role of YTHDF3 in OS progression, an array of *in vitro* and *in vivo* assays were conducted. YTHDF3 significantly promoted

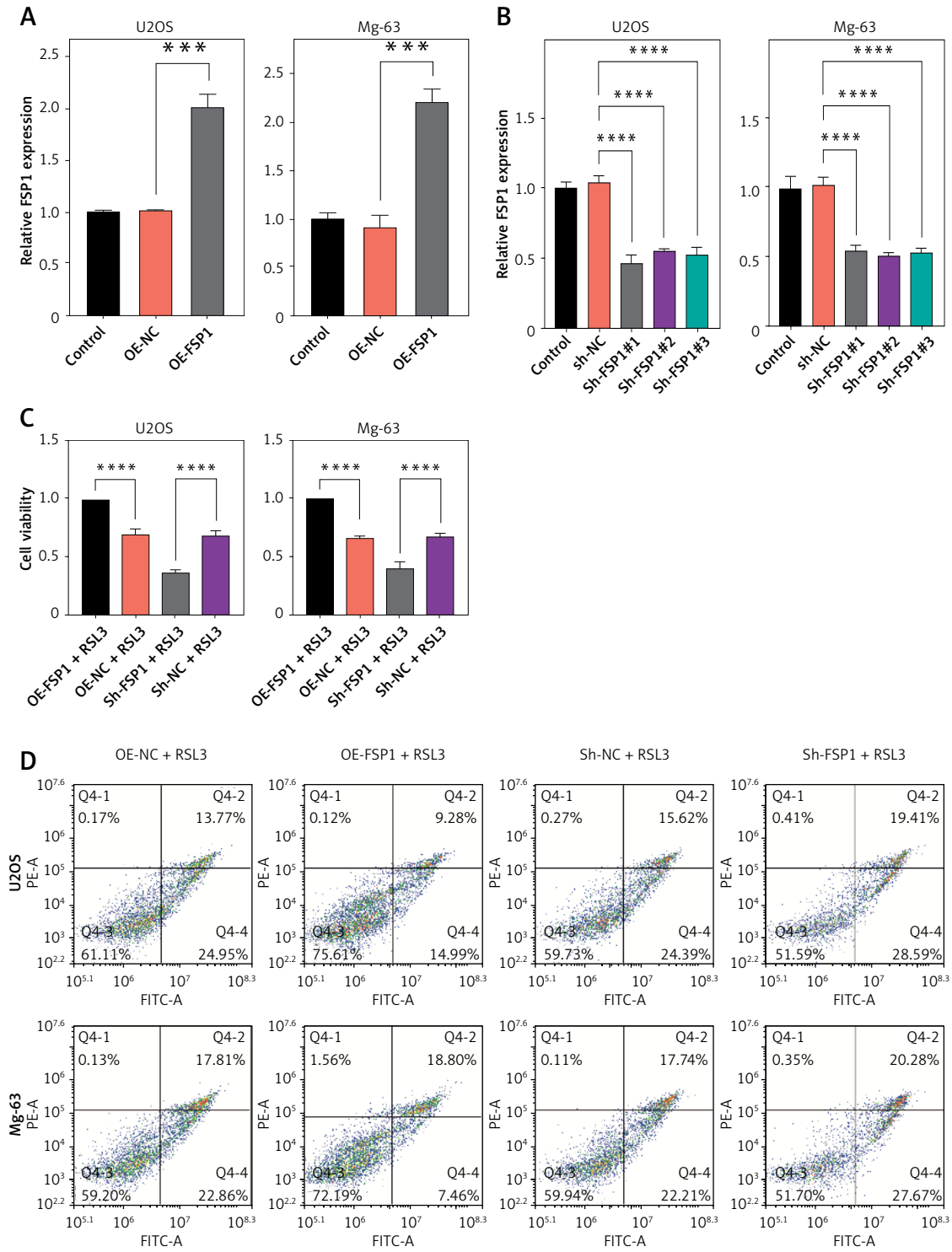

Figure 5. Influence of FSP1 modulation on ferroptosis susceptibility in OS cells. **A**, **B** – Lentivirus introduced FSP1 targeting (shFSP1) and FSP1 gene carrying (OE-FSP1) constructs in U2OS and Mg-63 cells, confirmed by qRT-PCR for knockdown and overexpression efficiency. **C** – CCK-8 assays show proliferation differences between OE-FSP1 and OE-NC, as well as shFSP1 and Sh-NC cells. **D** – Flow cytometry-based apoptosis analysis reveals varying rates in OE-FSP1 and shFSP1 cells

***P < 0.01, ***p < 0.001, ****p < 0.0001.*

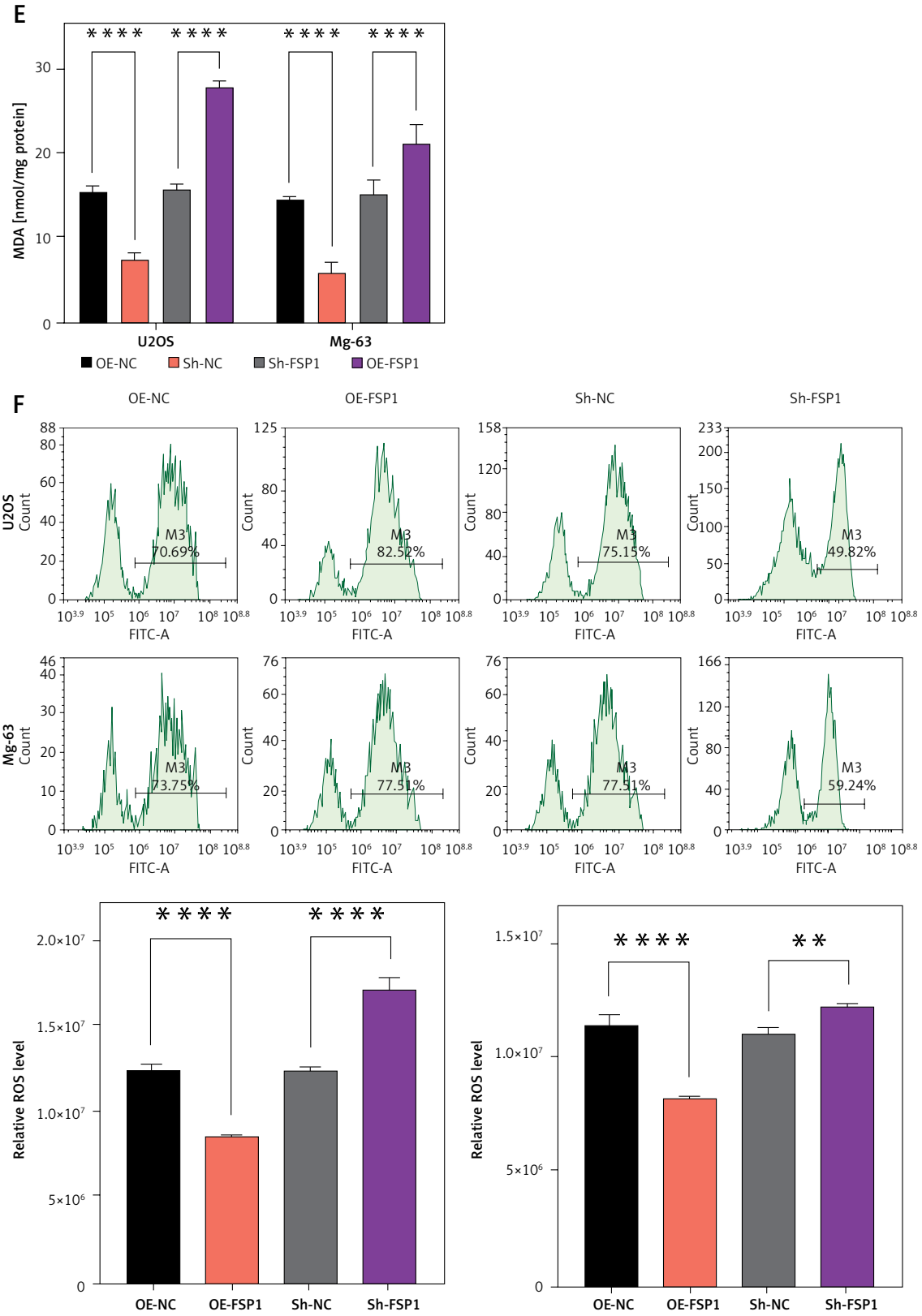

Figure 5. Cont. **E** – ELISA indicates MDA level changes upon FSP1 overexpression and knockdown. **F** – Flow cytometry analysis demonstrates ROS level alterations with FSP1 manipulation

***P < 0.01, ***p < 0.001, ****p < 0.0001.*

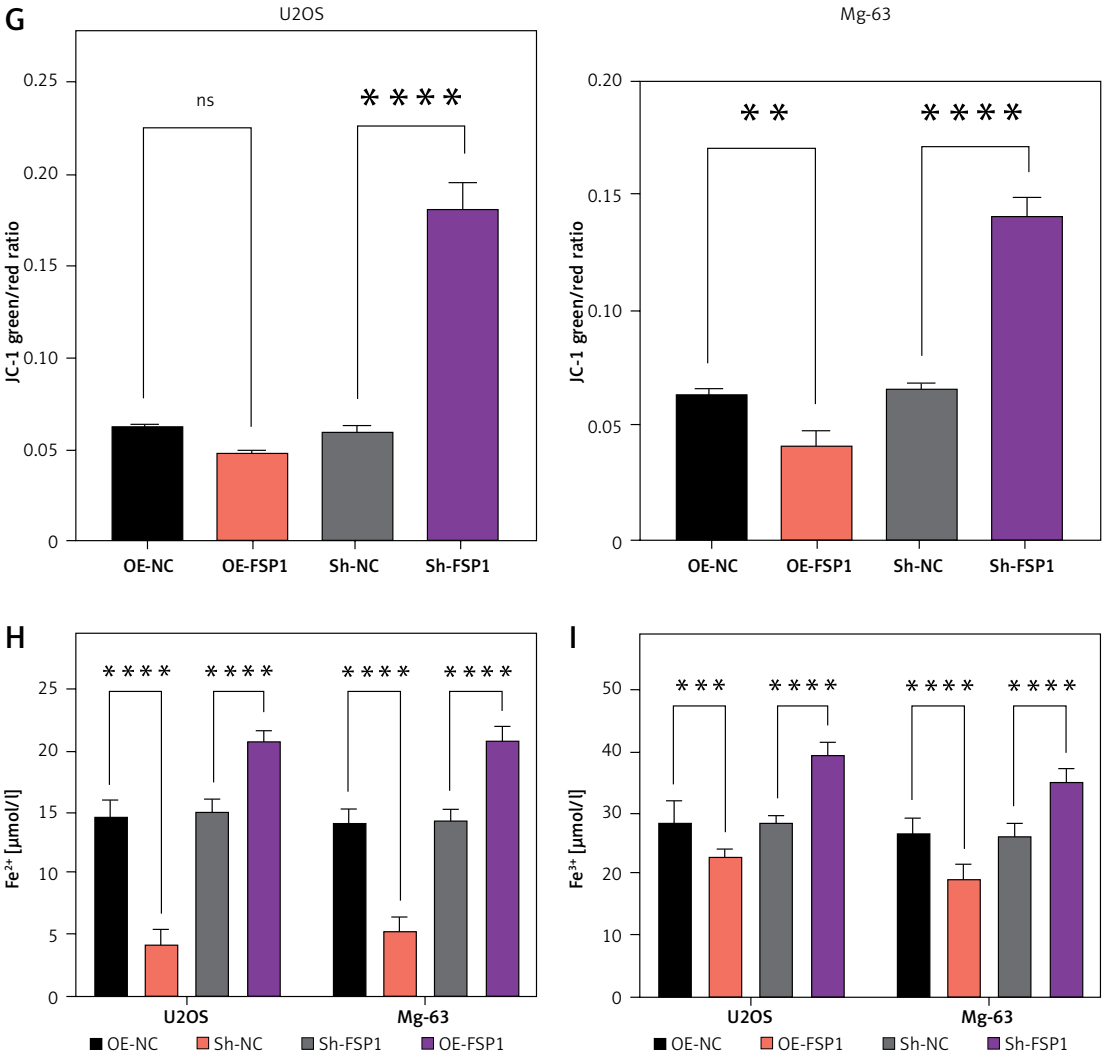

Figure 5. Cont. **G** – JC-1 staining reflects mitochondrial membrane potential changes caused by FSP1 modulation. **H**, **I** – FSP1's impact on cellular Fe^{2+} and Fe^{3+} levels is observed through iron assay kit

***P < 0.01, ***p < 0.001, ****p < 0.0001.*

cell proliferation while suppressing apoptosis in OS cells. MDA, an end-product of lipid peroxidation, emerges as both a biomarker and contributor to ferroptosis cascades, amplifying oxidative stress and ultimately driving cellular demise [41, 42]. Meanwhile, ROS, with their dual role as signaling molecules and oxidative agents, intricately participate in propagating lipid peroxidation and disrupting redox equilibrium, thereby orchestrating ferroptosis [43]. Disturbances in mitochondrial membrane potential potentiate iron-induced cytotoxicity by disrupting energy homeostasis and redox signaling, playing a pivotal role in the early events of ferroptosis [44]. Elevated iron levels fuel the Fenton reaction, fostering ROS generation and lipid peroxidation, thereby exacerbating the ferroptosis response [45]. Our study revealed that YTHDF3 is capable of suppressing levels of MDA, ROS, and iron ions in OS cells, raising mitochondrial membrane potential, inhibiting ferroptosis, and thereby promoting OS progression.

In the realm of ferroptosis, the roles of FSP1 and GPX4 have garnered substantial attention for their pivotal involvement in orchestrating cellular demise pathways. FSP1, a recently identified protein, has emerged as a critical sentinel in counteracting ferroptosis cell death [46, 47]. It functions as an indispensable constituent of the CoQ10 (coenzyme Q10) biosynthesis pathway, thereby facilitating the reduction of lipid peroxides and preserving the integrity of cellular membranes [48, 49]. Conversely, GPX4, a selenoenzyme, occupies a central position in defense against ferroptosis insults, intercepting the perilous cascade of lipid peroxidation [50]. In concert, the coordinated activities of FSP1 and GPX4 finely tune a defensive mechanism to combat ferroptosis [51]. Notably, levels of FSP1 and GPX4 are significantly elevated

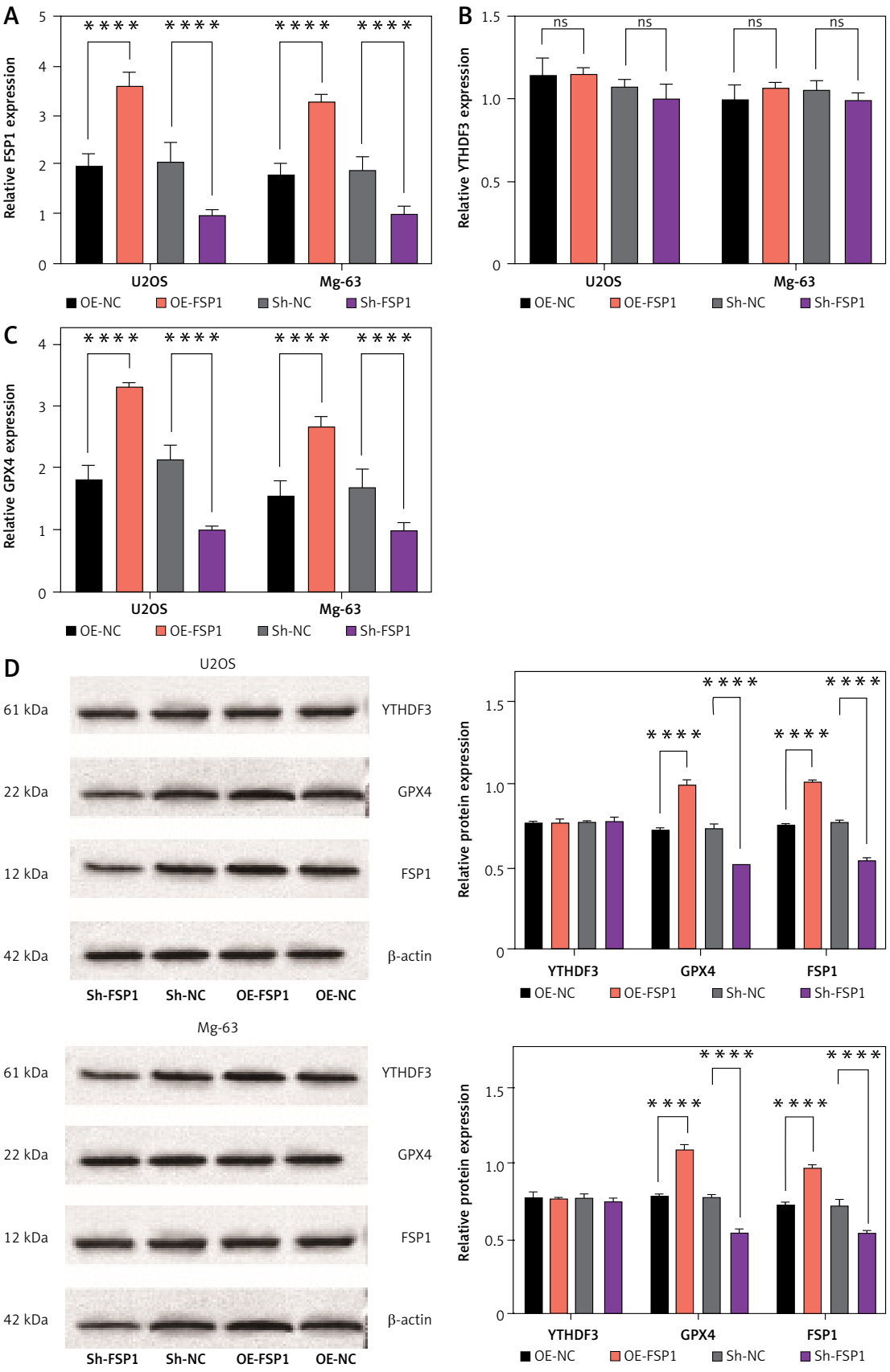

Figure 6. Impact of FSP1 modulation on GPX4 levels and ferroptosis susceptibility in OS cells. **A**–**D** – qRT-PCR and Western blot confirm FSP1's regulation of YTHDF3 and GPX4 in OS cells

*****P < 0.0001.*

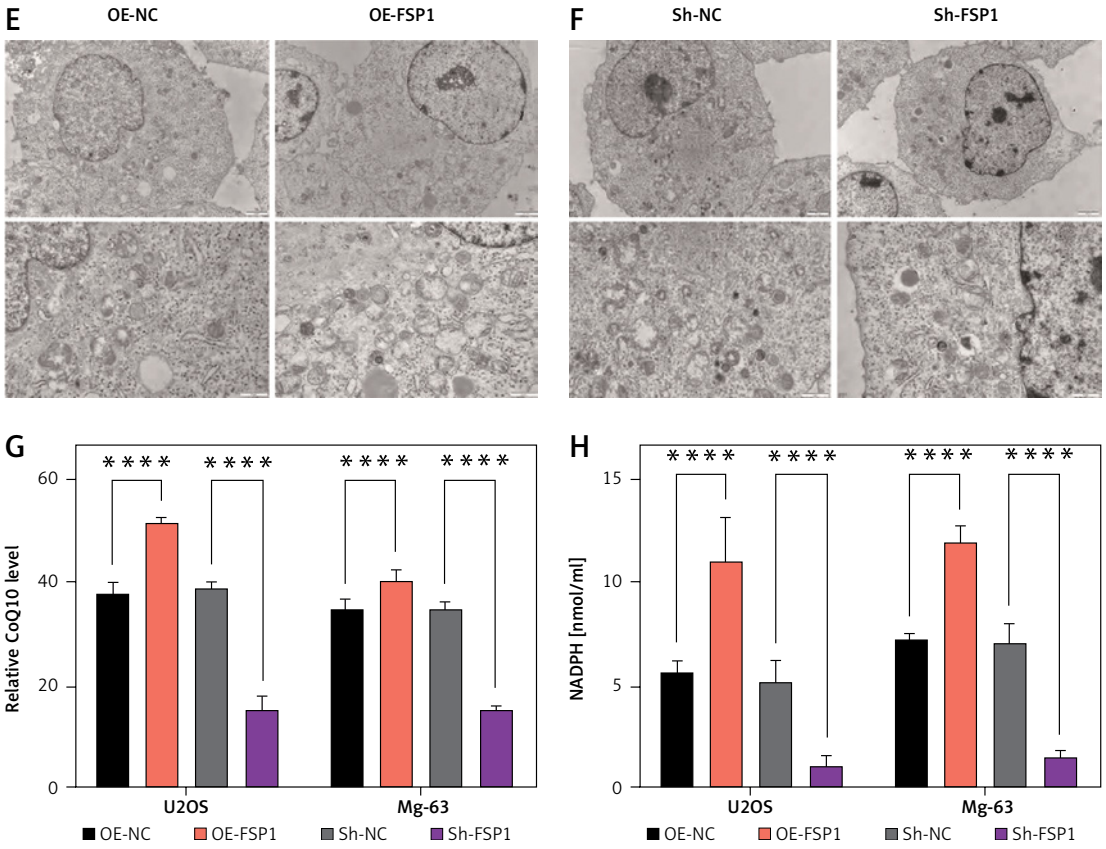

Figure 6. Cont. **E** – Transmission electron microscopy images reveal FSP1 overexpression's counteraction of RSL3-induced ferroptosis-associated morphological changes. **F** – Transmission electron microscopy images depict FSP1 knockdown's attenuation of RSL3-induced ferroptosis-associated morphological alterations. CoQ10 (**G**) and NADPH (**H**) levels were determined upon FSP1 overexpression and knockdown

*****P < 0.0001.*

in OS tissues. Cell assays verified that knockdown of YTHDF3 substantially down-regulated GPX4 and FSP1 levels. Furthermore, induction by RSL3 significantly diminished the m6A methylation of FSP1 in OS cells. Overexpression of FSP1 in OS cells was found to bolster cell proliferation, inhibit apoptosis, and concurrently restrain iron-mediated cell death. Collectively, these data corroborate the potential downstream targeting of FSP1 by YTHDF3 in OS.

In recent years, the role of ferroptosis suppressor protein (FSP) in cancer research has garnered substantial attention, emerging as a critical player in cancer progression and malignancy [51, 52]. FSP1 has been implicated in various aspects of tumor development, including metastasis, epithelial-mesenchymal transition (EMT), and tumor-stroma interactions [53, 54]. Notably, its involvement in cancer-related processes is linked to its regulatory role in N6-methyladenosine (m6A) RNA modification, a pivotal post-transcriptional mechanism influencing gene expression [55, 56]. For instance, a pioneering study by Song *et al.* revealed that exosomal miR-4443, regulated by METTL3 via m6A modification, mediates ferroptosis by modulating FSP1 expression, thereby promoting cisplatin resistance in NSCLC [8]. Similarly, another study by Bu *et al.* stabilized FSP1 mRNA through m6A modification, thereby inhibiting ferroptosis and driving glioma progression [57]. These findings accentuate the importance of FSP1 as an m6A-modified gene in diverse cancer types. In this study, stability analyses demonstrated that inhibiting YTHDF3 significantly compromised the stability of FSP1 mRNA in OS cells, further confirming YTHDF3's ability to enhance the stability of FSP1 mRNA. Functional rescue experiments validated the impact of the YTHDF3/FSP1 axis on OS. Knockdown of YTHDF3 induced decreased proliferation and ferroptosis, both of which could be rescued by FSP1 overexpression. Furthermore, FSP1 overexpression partially restored the downregulation of CoQ10 and NADPH caused by YTHDF3 knockdown. Collectively, these results suggest that YTHDF3 may promote FSP1 mRNA translation in an m6A-dependent manner, thereby inhibiting ferroptosis through the FSP1-CoQ10-NADPH pathway and promoting OS progression.

In conclusion, we investigated the pivotal roles played by YTHDF3 and FSP1 in regulation of

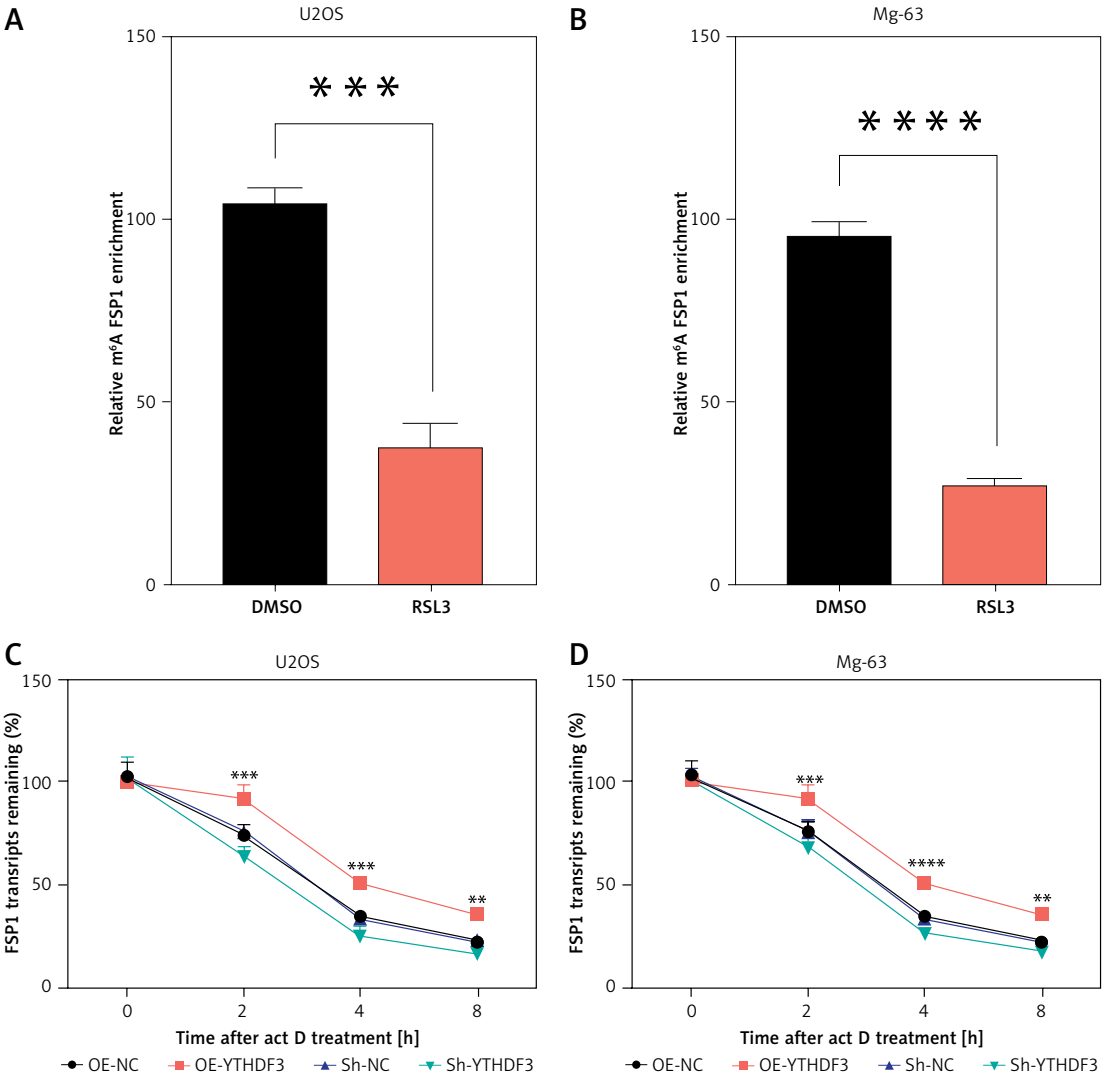

Figure 7. YTHDF3-mediated m6A modification of FSP1 modulates ferroptosis in OS. **A**, **B** – RSL3-induced treatment alters FSP1 m6A methylation in OS cells, measured by EpiQuik m6A RNA Methylation Quantitative Assay Kit. **C** – YTHDF3 overexpression affects FSP1 mRNA levels following Act D treatment, observed through RNA decay analyses. **D** – YTHDF3 silencing influences FSP1 mRNA levels upon Act D treatment

***P < 0.01, ***p < 0.001, ****p < 0.0001.*

the CoQ10-GAPDH axis and ferroptosis in OS. Initially, we established a ferroptosis model in U2OS and Mg-63 cells through treatment with RSL3. Our findings revealed that the overexpression of YTHDF3 exerted a mitigating effect on ferroptosis, whereas its knockdown intensified this cellular process. Notably, FSP1 emerged as a key mediator of YTHDF3's regulatory impact. Mechanistically, YTHDF3 enhanced the stability and translation of m6a-modified FSP1 mRNA and altered CoQ10 and GAPDH levels to regulate ferroptosis. This study not only enhances our understanding of ferroptosis regulation but also sheds light on the significance of YTHDF3 and FSP1 as potential targets for therapeutic intervention in OS, offering new prospects for cancer treatment strategies.

Acknowledgments

This work is the result of a collaborative effort by Wei Liu and Qingning Li.

Funding

This study was supported by the Research Fund of Anhui Institute of Translational Medicine (No. 2023zhyx-C74) and the University Natural Science Foundation of Anhui Province (No. 2023AH053173).

Ethical approval

The Ethics Committee of The Second Hospital Affiliated with Anhui Medical University approved the study in accordance with ethical standards (No. SL-YX[YS]2023-019).

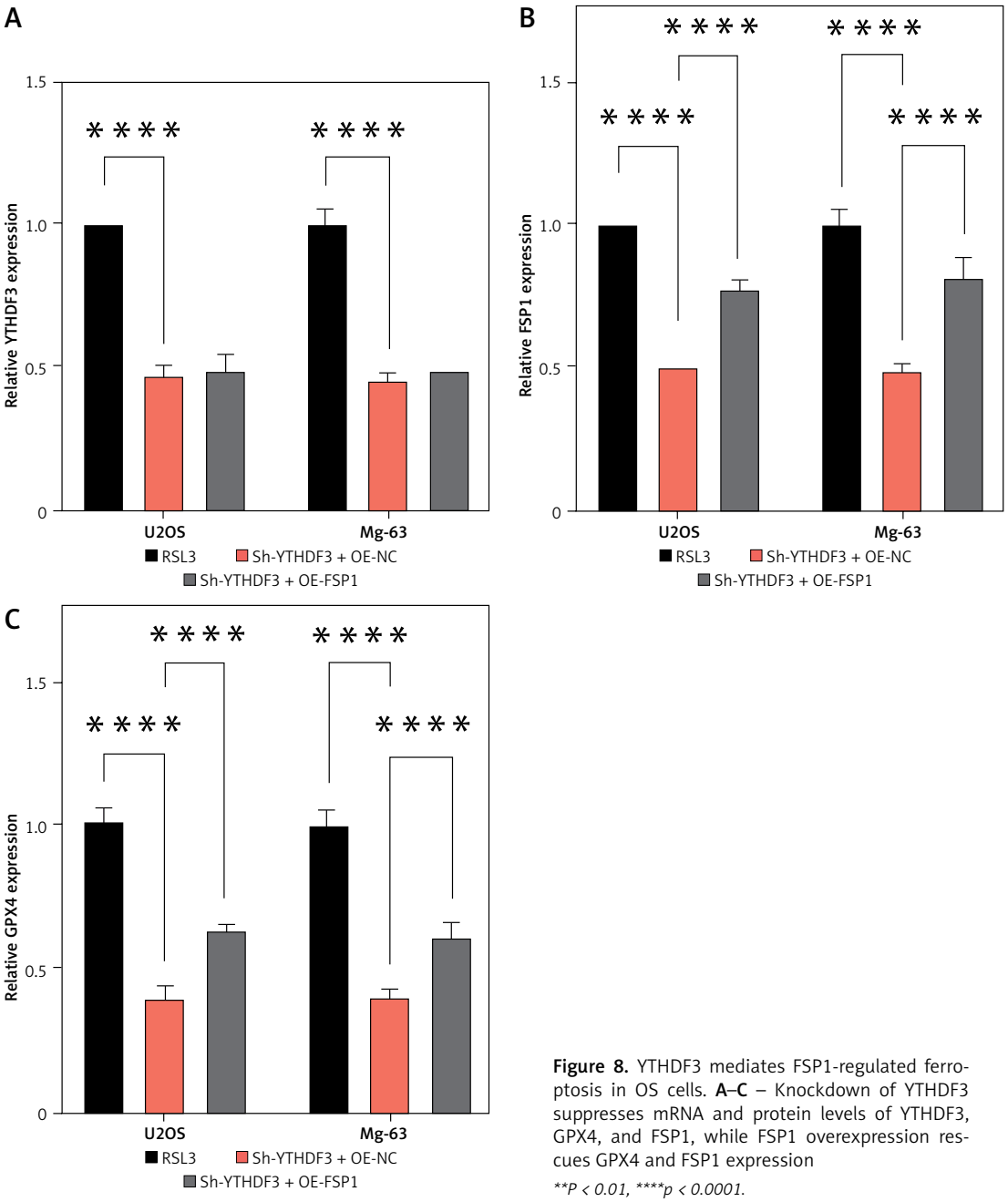

Figure 8. YTHDF3 mediates FSP1-regulated ferroptosis in OS cells. **A–C** – Knockdown of YTHDF3 suppresses mRNA and protein levels of YTHDF3, GPX4, and FSP1, while FSP1 overexpression rescues GPX4 and FSP1 expression

***P < 0.01, ****p < 0.0001.*

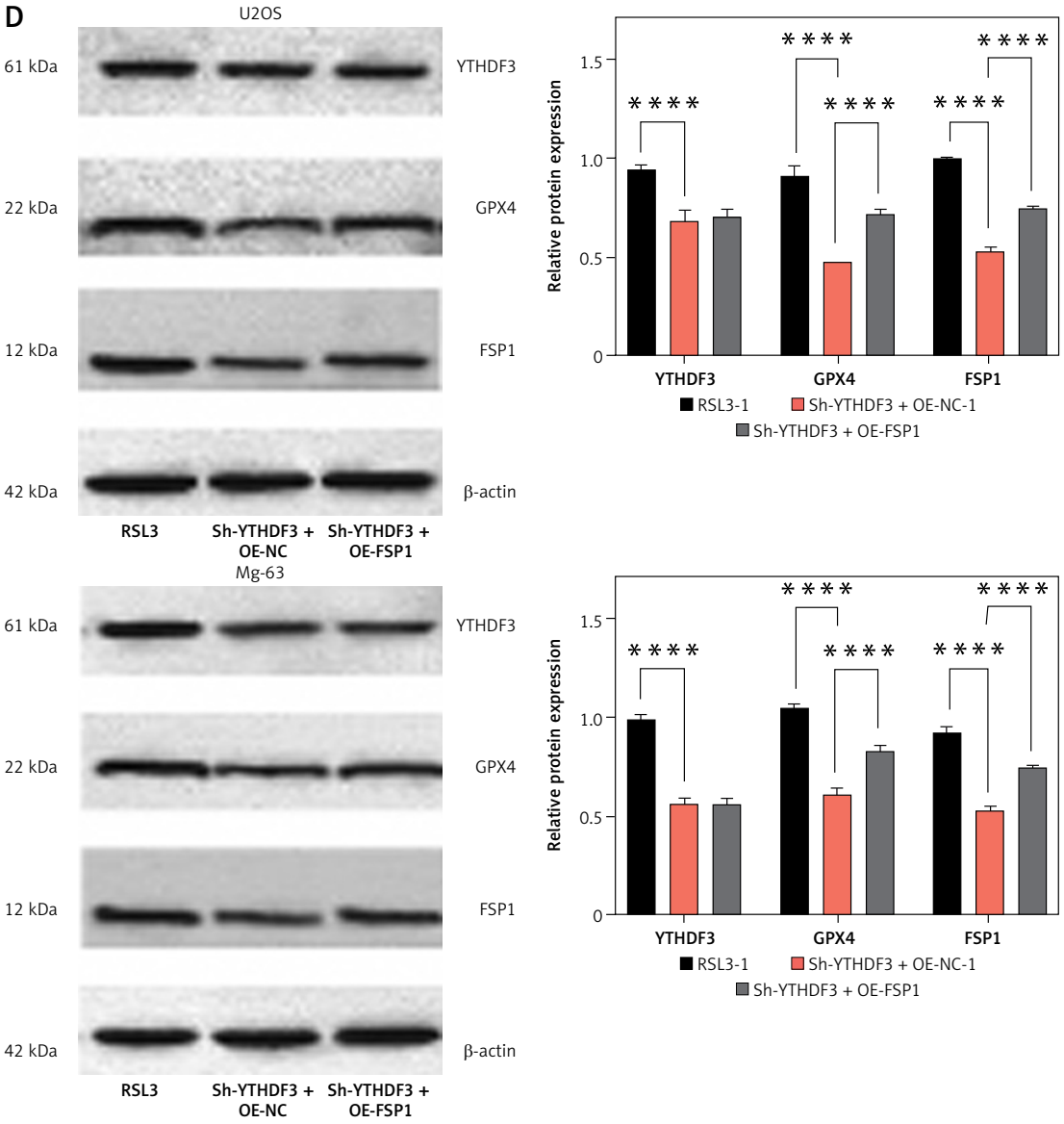

Figure 8. Cont. **D** – Knockdown of YTHDF3 suppresses mRNA and protein levels of YTHDF3, GPX4, and FSP1, while FSP1 overexpression rescues GPX4 and FSP1 expression. **E** – sh-YTHDF3 inhibits proliferation and induces apoptosis, which is reversed by FSP1 overexpression

***P < 0.01, ****p < 0.0001.*

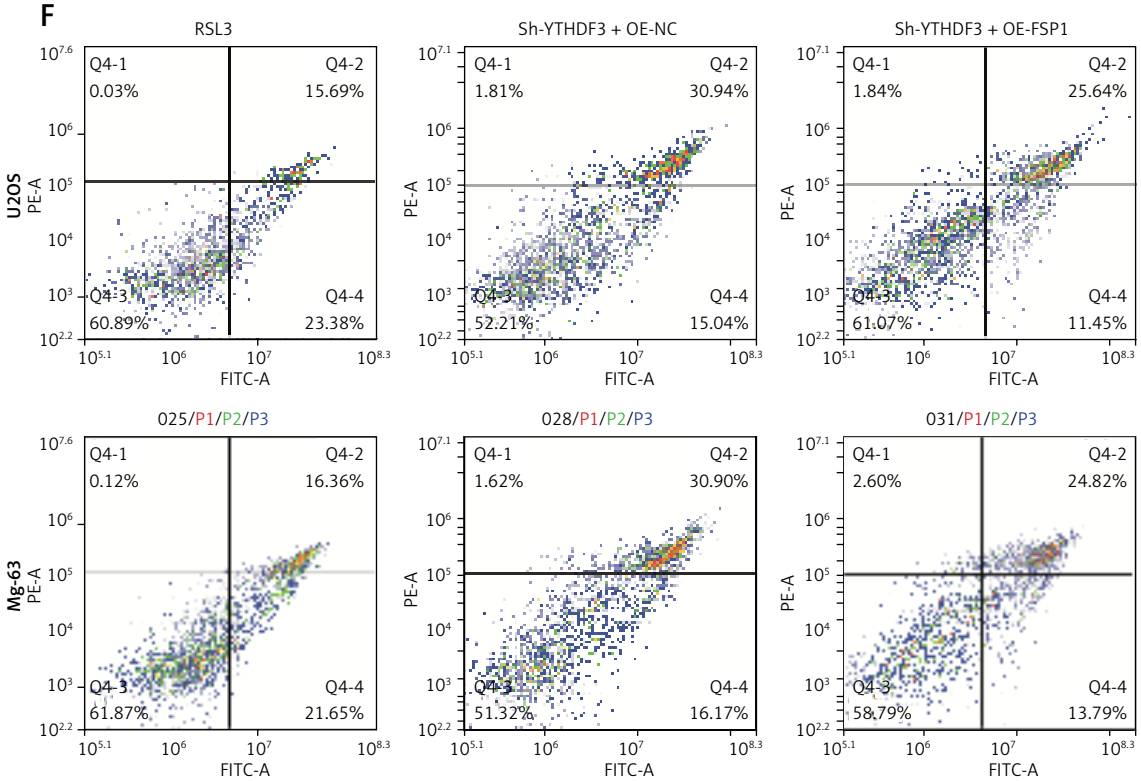

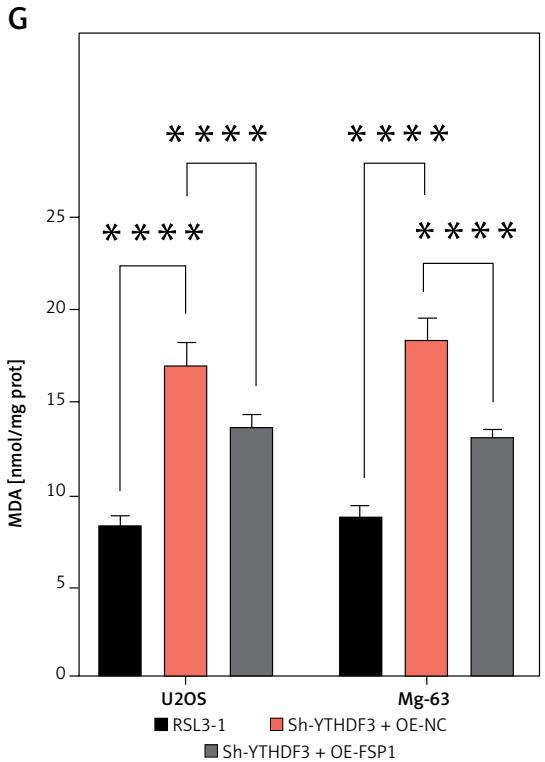

Figure 8. Cont. **F** – Quantification of apoptotic cells. **G** – FSP1 overexpression attenuates accumulation of MDA, ROS, Fe^{2+}, and Fe^{3+} induced by sh-YTHDF3

***P < 0.01, ****p < 0.0001.*

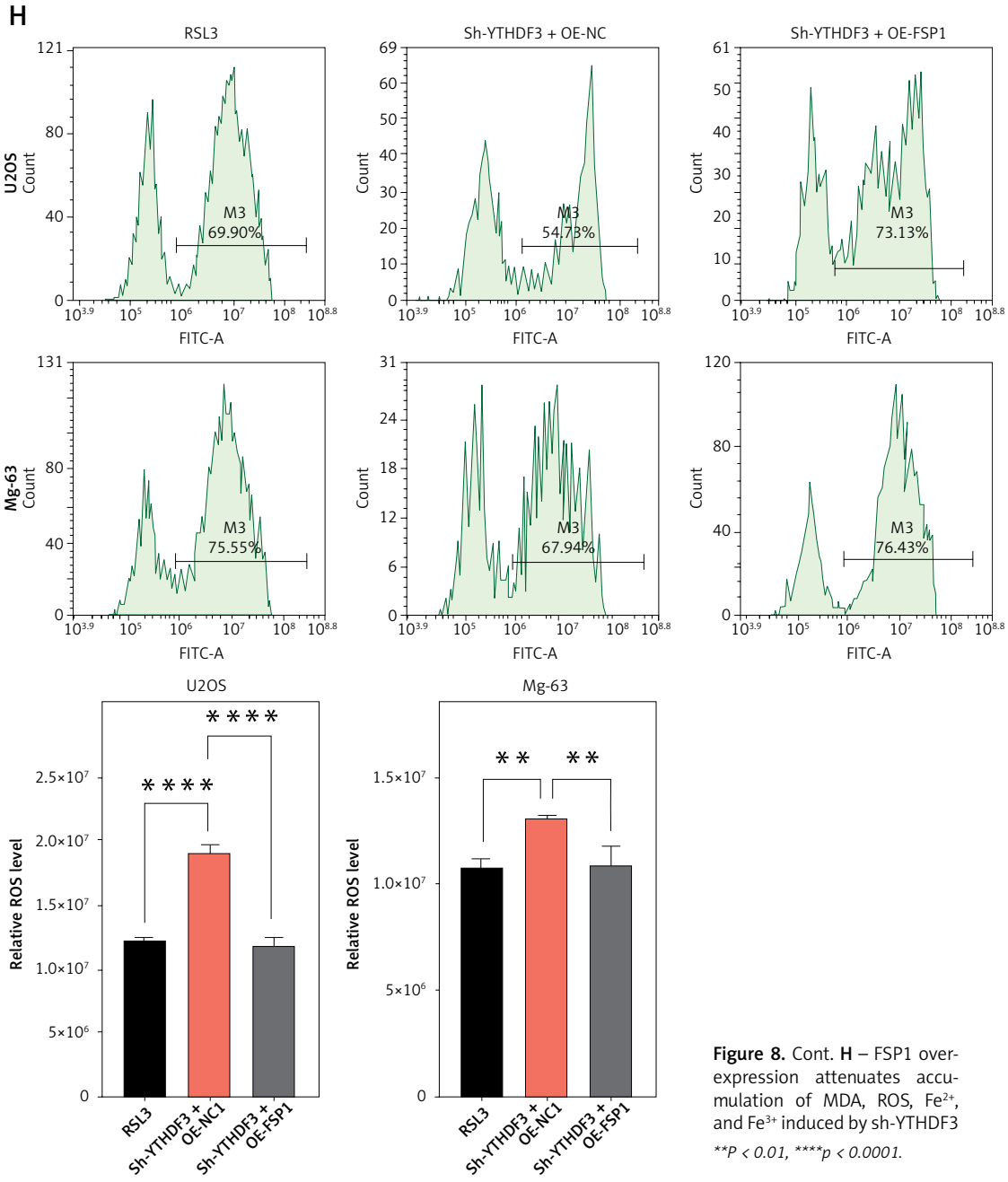

Figure 8. Cont. **H** – FSP1 overexpression attenuates accumulation of MDA, ROS, Fe^{2+}, and Fe^{3+} induced by sh-YTHDF3

***P < 0.01, ****p < 0.0001.*

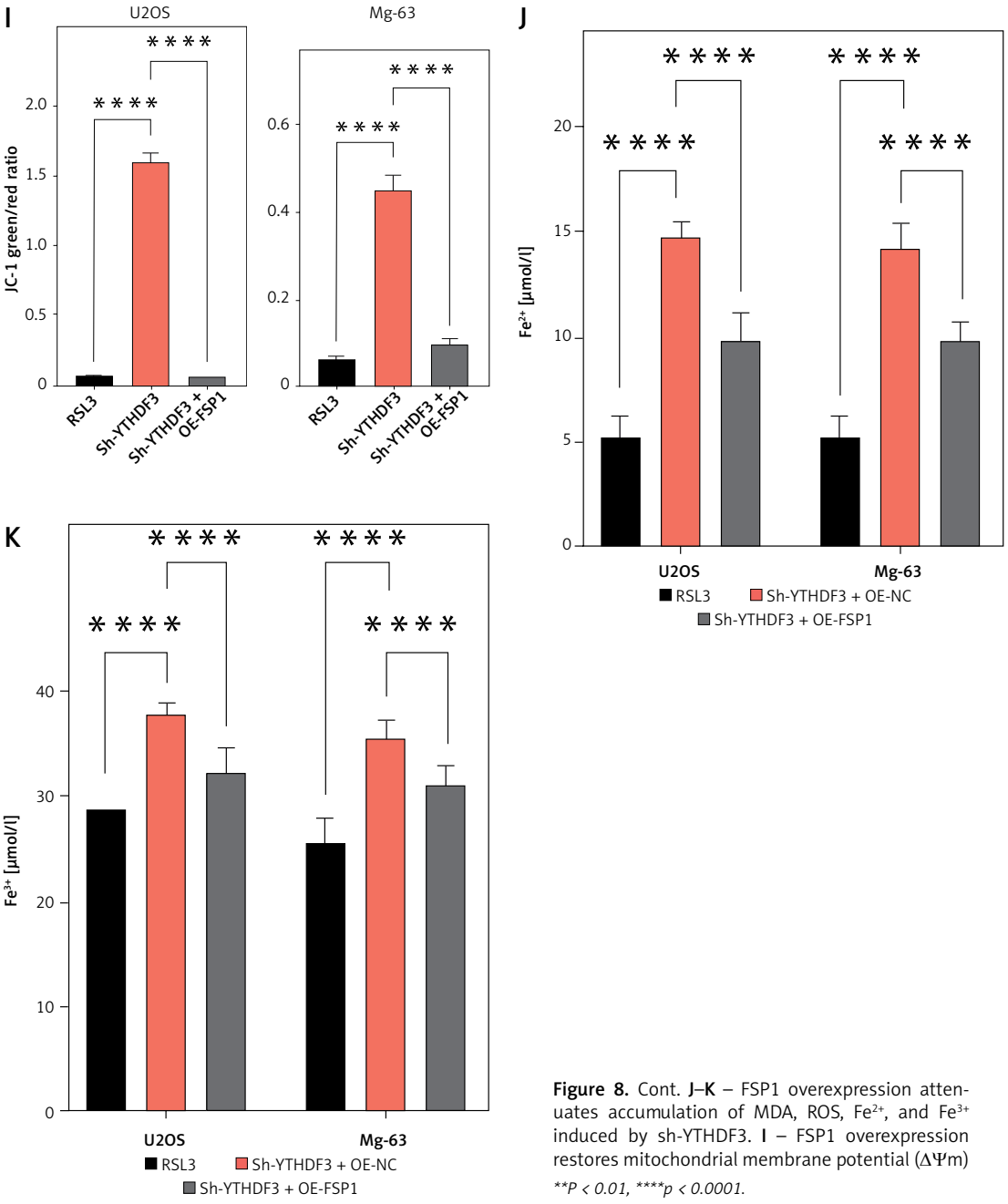

Figure 8. Cont. **J–K** – FSP1 overexpression attenuates accumulation of MDA, ROS, Fe^{2+}, and Fe^{3+} induced by sh-YTHDF3. **I** – FSP1 overexpression restores mitochondrial membrane potential ($\Delta\Psi m$)
***P < 0.01, ****p < 0.0001.*

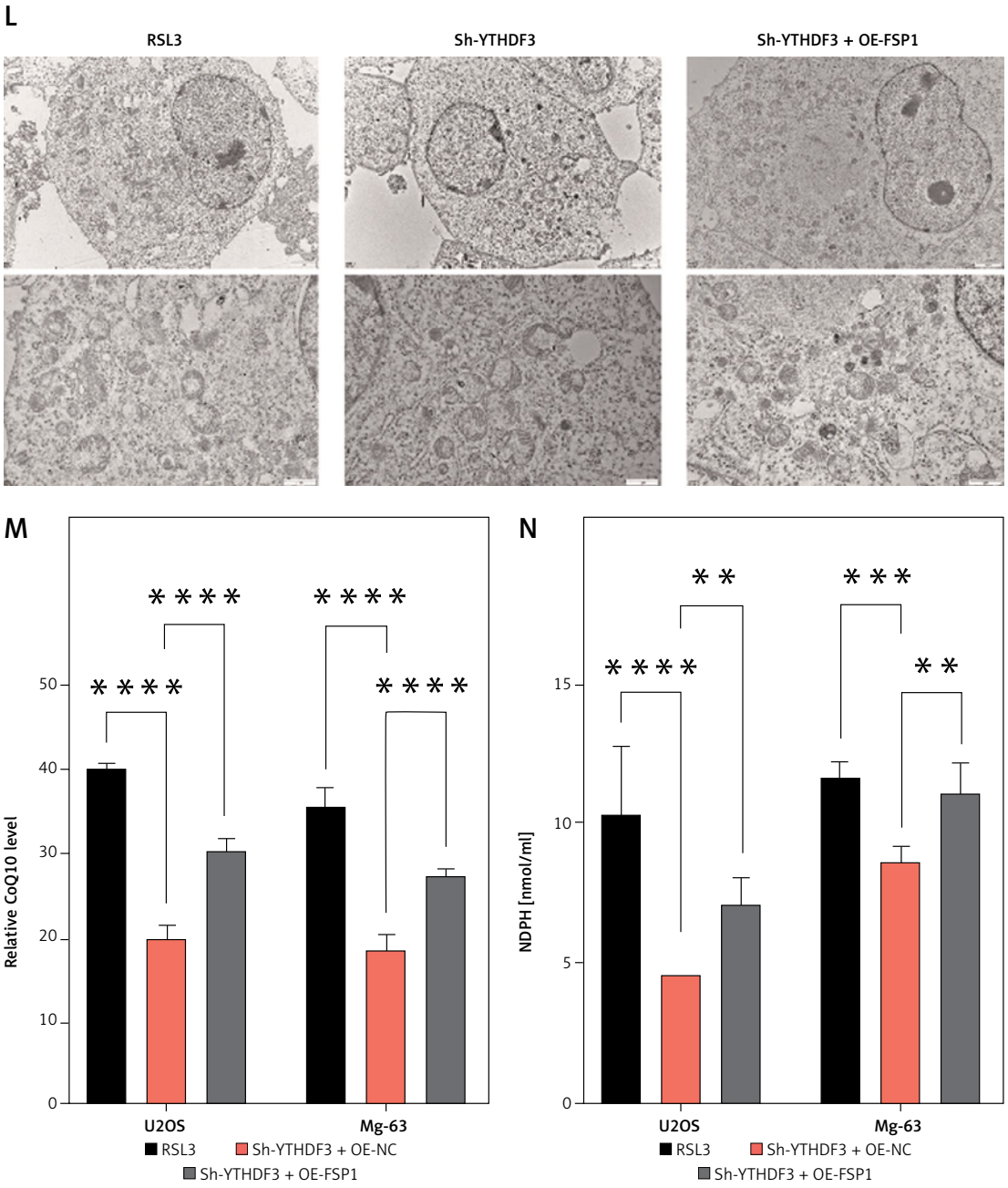

Figure 8. Cont. **L** – Transmission electron microscopy images show mitochondrial morphology (yellow arrows) and chromatin condensation (white arrows). **M**, **N** – sh-YTHDF3 inhibits CoQ10 and NADPH levels, which are rescued by FSP1 overexpression

***P < 0.01, ****p < 0.0001.*

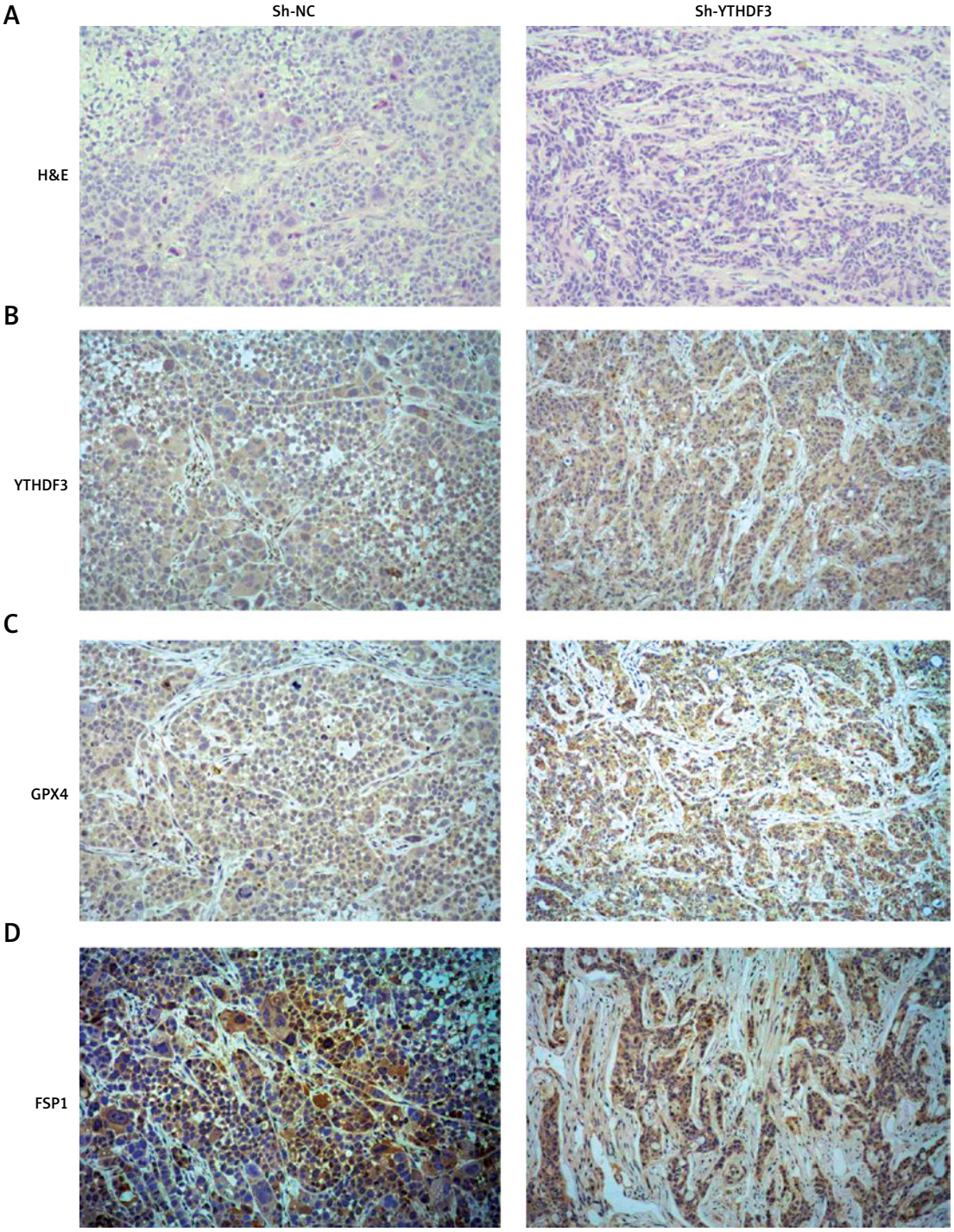

Figure 9. Implications of YTHDF3 in regulating FSP1-CoQ10-NADPH axis and ferroptosis. **A** – Histopathological analysis of sh-YTHDF3 U2OS cell xenografts in mice, revealing altered tumor pathology compared to the control group. **B–D** – Immunohistochemical staining illustrating YTHDF3 knockdown's impact on YTHDF3, GPX4, and FSP1 expression in tumor tissues

****P < 0.001, ****p < 0.0001.*

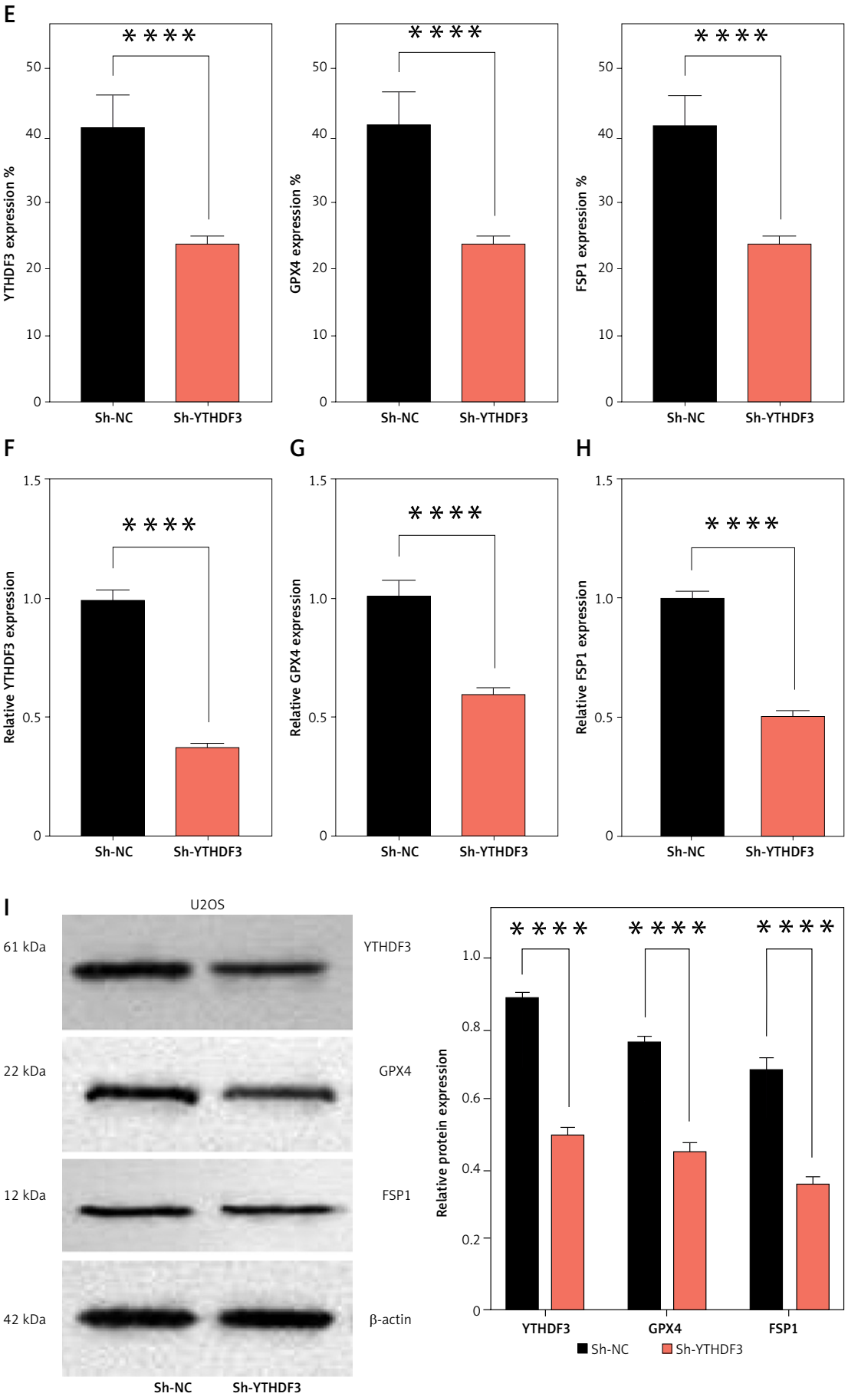

Figure 9. Cont. **E** – Immunohistochemical staining illustrating YTHDF3 knockdown's impact on YTHDF3, GPX4, and FSP1 expression in tumor tissues. **F–I** – qRT-PCR and Western blot analyses confirming YTHDF3 knockdown's influence on FSP1 and GPX4 mRNA and protein levels in tumor samples

****P < 0.001, ****p < 0.0001.*

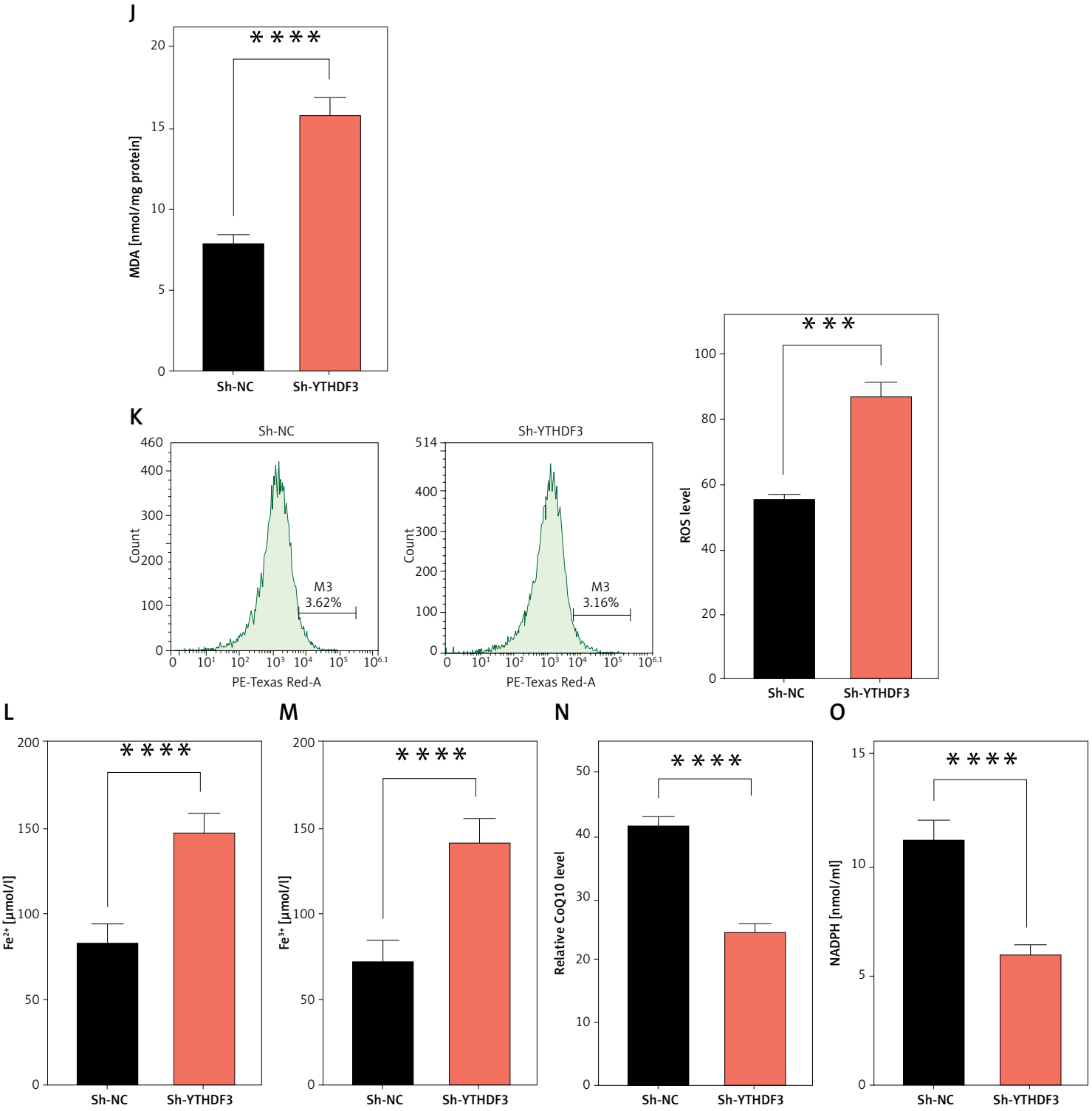

Figure 9. Cont. **J–O** – Quantification of MDA, ROS, Fe^{2+}, Fe^{3+}, CoQ10, and NADPH levels in tumor tissue after YTHDF3 knockdown

****P < 0.001, ****p < 0.0001.*

Conflict of interest

The authors declare no conflict of interest.

References

1. Nørregaard KS, Jürgensen HJ, Gårdsvoll H, Engelholm LH, Behrendt N, Søe K. Osteosarcoma and metastasis associated bone degradation - a tale of osteoclast and malignant cell cooperativity. Int J Mol Sci 2021; 22: 6865.
2. Zhao Z, Lin X, Tong Y, Li W. Silencing lncRNA ZFAS1 or elevated microRNA-135a represses proliferation, migration, invasion and resistance to apoptosis of osteosarcoma cells. Cancer Cell Int 2019; 19: 326.
3. Kudarha R, Dhas N, Mutalik S. Distinct features of iron based metal organic frameworks (MOFs) for ferroptosis mediated cancer therapy: a comprehensive review. Coord Chem Rev 2023; 494: 215330.
4. Lin KJ, Chen SD, Lin KL, et al. Iron brain menace: the involvement of ferroptosis in Parkinson disease. Cells 2022; 11: 3829.
5. Lee J, Roh JL. Unleashing ferroptosis in human cancers: targeting ferroptosis suppressor protein 1 for overcoming therapy resistance. Antioxidants 2023; 12: 1218.
6. Guo J, Chen L, Ma M. Ginsenoside Rg1 suppresses ferroptosis of renal tubular epithelial cells in sepsis-induced acute kidney injury via the FSP1-CoQ10-NAD (P) H pathway. Curr Med Chem 2023; 31: 2119-32.
7. Li W, Liang L, Liu S, Yi H, Zhou Y. FSP1: a key regulator of ferroptosis. Trends Mol Med 2023; 29: 753-64.
8. Song Z, Jia G, Ma P, Cang S. Exosomal miR-4443 promotes cisplatin resistance in non-small cell lung carcinoma by regulating FSP1 m6A modification-mediated ferroptosis. Life Sci 2021; 276: 119399.
9. Sun Y, Jin D, Zhang Z, et al. N6-methyladenosine (m6A) methylation in kidney diseases: mechanisms and therapeutic potential. Biochim Biophys Acta Gene Regul Mech 2023; 1886: 194967.
10. Chen D, Cheung H, Lau HCH, Yu J, Wong CC. N6-methyladenosine RNA-binding protein YTHDF1 in gastrointestinal cancers: function, molecular mechanism and clinical implication. Cancers 2022; 14: 3489.
11. Chang LL, Xu QG, Liu XL, et al. Emerging role of m6A methylation modification in ovarian cancer. Cancer Cell Int 2021; 21: 663.
12. Yang Z, Cai Z, Yang C, Luo Z, Bao X. ALKBH5 regulates Stat3 activity to affect the proliferation and tumorigenicity of osteosarcoma via an m6A-YTHDF2-dependent manner. eBioMedicine 2022; 80: 104019.
13. Li HB, Huang G, Tu J, et al. METTL14-mediated epitranscriptome modification of MN1 mRNA promote tumorigenicity and all-trans-retinoic acid resistance in osteosarcoma. EBioMedicine 2022; 82: 104142.
14. Xu Y, Zhang W, Shen F, et al. YTH domain proteins: a family of m6A readers in cancer progression. Front Oncol 2021; 11: 629560.
15. Yu Y, Meng LL, Chen XY, et al. m6A reader YTHDF3 is associated with clinical prognosis, related RNA signatures and immunosuppression in gastric cancer. Cell Signal 2023; 108: 110699.
16. Ni W, Yao S, Zhou Y, et al. Long noncoding RNA GAS5 inhibits progression of colorectal cancer by interacting with and triggering YAP phosphorylation and degradation and is negatively regulated by the m6A reader YTHDF3. Mol Cancer 2019; 18: 143.
17. Pillai-Kastoori L, Schutz-Geschwender AR, Harford JA. A systematic approach to quantitative Western blot analysis. Anal Biochem 2020; 593: 113608.
18. Li S, He Y, Chen K, et al. RSL3 drives ferroptosis through NF-κB pathway activation and GPX4 depletion in glioblastoma. Oxid Med Cell Longev 2021; 2021: 2915019.
19. Wang DP, Tang XZ, Liang QK, et al. microRNA-599 promotes apoptosis and represses proliferation and epithelial-mesenchymal transition of papillary thyroid carcinoma cells via downregulation of Hey2-depentent Notch signaling pathway. J Cell Physiol 2020; 235: 2492-505.
20. Zeng F, Ye l, Zhou Q, et al. Inhibiting SCD expression by IGF1R during lorlatinib therapy sensitizes melanoma to ferroptosis. Redox Biol 2023; 61: 102653.
21. Chen Y, Chen Y, Zhang H, Wang T. Pterostilbene as a protective antioxidant attenuates diquat-induced liver injury and oxidative stress in 21-day-old broiler chickens. Poult Sci 2020; 99: 3158-67.
22. Ma Y, Li Y, Ling S, et al. Loss of heterozygosity for KrasG12D promotes REDD1-dependent, non-canonical glutamine metabolism in pancreatic ductal adenocarcinoma. Biochem Biophys Res Commun 2020; 526: 880-8.
23. Chai Y, Cao ZM, Yu R, et al. Dexmedetomidine attenuates LPS-induced monocyte-endothelial adherence via inhibiting Cx43/PKC-α/NOX2/ROS signaling pathway in monocytes. Oxid Med Cell Longev 2020; 2020: 2930463.
24. Nikaido Y, Midorikawa Y, Furukawa T, et al. The role of neutrophil gelatinase-associated lipocalin and iron homeostasis in object recognition impairment in aged sepsis-survivor rats. Sci Rep 2022; 12: 249.
25. Deng X, Yang P, Gao T, Liu M, Li X. Allicin attenuates myocardial apoptosis, inflammation and mitochondrial injury during hypoxia-reoxygenation: an in vitro study. BMC Cardiovasc Disord 2021; 21: 200.
26. Bornaque F, Delannoy CP, Courty E, et al. Glucose regulates m6A methylation of RNA in pancreatic Islets. Cells 2022; 11: 291.
27. Xia P, Zhang H, Xu K, et al. MYC-targeted WDR4 promotes proliferation, metastasis, and sorafenib resistance by inducing CCNB1 translation in hepatocellular carcinoma. Cell Death Dis 2021; 12: 691.
28. Park KR, Yun HM, Hong JT. G721-0282 inhibits cell growth and induces apoptosis in human osteosarcoma through down-regulation of the STAT3 pathway. Int J Biol Sci 2020; 16: 330.
29. Chlipala E, Bendzinski CM, Chu K, et al. Optical density-based image analysis method for the evaluation of hematoxylin and eosin staining precision. J Histotechnol 2020; 43: 29-37.
30. Handbook of Practical Immunohistochemistry: Frequently Asked Questions. Lin F, Prichard JW, Liu H, Wilkerson ML (eds.). Springer Nature 2022
31. Sekhar KR, Hanna DN, Cyr S, et al. Glutathione peroxidase 4 inhibition induces ferroptosis and mTOR pathway suppression in thyroid cancer. Sci Rep 2022; 12: 19396.
32. Song T, Yang Y, Jiang S, Peng J. Novel insights into adipogenesis from the perspective of transcriptional and RNA N6-methyladenosine-mediated post-transcriptional regulation. Adv Sci 2020; 7: 2001563.
33. Fu Y, Dominissini D, Rechavi G, He C. Gene expression regulation mediated through reversible m6A RNA methylation. Nat Rev Genet 2014; 15: 293-306.

34. Meyer KD. m6A-mediated translation regulation. Biochim Biophys Acta Gene Regul Mechan 2019; 1862: 301-9.
35. Panneerdoss S, Eedunuri VK, Yadav P, et al. Cross-talk among writers, readers, and erasers of m6A regulates cancer growth and progression. Sci Adv 2018; 4: eaar8263.
36. He C, He C. m6A RNA methylation: from mechanisms to therapeutic potential. EMBO J 2021; 40: e105977.
37. Zaccara S, Jaffrey SR. A unified model for the function of YTHDF proteins in regulating m6A-modified mRNA. Cell 2020; 181: 1582-95.
38. Liu T, Wei Q, Jin J, et al. The m6A reader YTHDF1 promotes ovarian cancer progression via augmenting EIF3C translation. Nucleic Acids Res 2020; 48: 3816-31.
39. Chang G, Shi L, Ye Y, et al. YTHDF3 induces the translation of m6A-enriched gene transcripts to promote breast cancer brain metastasis. Cancer Cell 2020; 38: 857-71.
40. Ran Y, Yan Z, Jiang B, Liang P. N6-methyladenosine functions and its role in skin cancer. Exp Dermatol 2023; 32: 4-12.
41. Chen X, Kang R, Kroemer G, Tang D. Organelle-specific regulation of ferroptosis. Cell Death Differ 2021; 28: 2843-56.
42. Chen X, Kang R, Kroemer G, Tang D. Ferroptosis in infection, inflammation, and immunity. J Exp Med 2021; 218: e20210518.
43. Zeng W, Long X, Liu PS, Xie X. The interplay of oncogenic signaling, oxidative stress and ferroptosis in cancer. Int J Cancer 2023; 153: 918-31.
44. Sun K, Zhi Y, Ren W, et al. The mitochondrial regulation in ferroptosis signaling pathway and its potential strategies for cancer. Biomed Pharmacother 2023; 169: 115892.
45. Battaglia AM, Chirillo R, Aversa I, et al. Ferroptosis and cancer: mitochondria meet the "iron maiden" cell death. Cells 2020; 9: 1505.
46. Bersuker K, Hendricks JM, Li Z, et al. The CoQ oxidoreductase FSP1 acts parallel to GPX4 to inhibit ferroptosis. Nature 2019; 575: 688-92.
47. Brown CW, Amante JJ, Chhoy P, et al. Prominin2 drives ferroptosis resistance by stimulating iron export. Dev Cell 2019; 51: 575-86.e4.
48. Zhao Y, Liu Y, Xu Y, et al. The role of ferroptosis in blood–brain barrier injury. Cell Mol Neurobiol 2023; 43: 223-36.
49. Luo M, Yan J, Hu X, et al. Targeting lipid metabolism for ferroptotic cancer therapy. Apoptosis 2023; 28: 81-107.
50. Su LJ, Zhang JH, Gomez H, et al. Reactive oxygen species-induced lipid peroxidation in apoptosis, autophagy, and ferroptosis. Oxid Med Cell Longev 2019; 2019: 5080843.
51. Doll S, Freitas FP, Shah R, et al. FSP1 is a glutathione-independent ferroptosis suppressor. Nature 2019; 575: 693-8.
52. Yang J, Jia Z, Zhang J, et al. Metabolic intervention nanoparticles for triple-negative breast cancer therapy via overcoming FSP1-mediated ferroptosis resistance. Adv Healthc Mater 2022; 11: 2102799.
53. Bornes L, van Scheppingen RH, Beerling E, et al. Fsp1-mediated lineage tracing fails to detect the majority of disseminating cells undergoing EMT. Cell Rep 2019; 29: 2565-9.e3.
54. Ni Y, Zhou X, Yang J, et al. The role of tumor-stroma interactions in drug resistance within tumor microenvironment. Front Cell Develop Biol 2021; 9: 637675.
55. Zhang Z, Wei W, Wang H, Dong J. N6-methyladenosine-sculpted regulatory landscape of noncoding RNA. Front Oncol 2021; 11: 743990.
56. Feng H, Yuan X, Wu S, et al. Effects of writers, erasers and readers within miRNA-related m6A modification in cancers. Cell Prolif 2023; 56: e13340.
57. Bu C, Hu S, Yu J, et al. Fear stress promotes glioma progression through inhibition of ferroptosis by enhancing FSP1 stability. Clin Transl Oncol 2023; 25: 1378-88.